BMC Chemistry

RESEARCH Open Access

Trifluoromethyl–pyrazole–carboxamides as COX inhibitors: synthesis, microed structural analysis, computational profiling, and biological evaluation

Mohammed Hawash[1*], Nisreen Shweiki[1], Mohammed T. Qaoud[2], Irfan Çapan[3,4], Murad Abualhasan[1], Anil Kumar[5], Barbara Olech[5] and Paulina Maria Dominiak[5]

Abstract

Background Non-steroidal anti-inflammatory drugs (NSAIDs) are among the most widely prescribed medications for the treatment of inflammation, pain, and fever, primarily acting as competitive inhibitors of the cyclooxygenase (COX) enzymes.

Objectives The present study aimed to design a series of trifluoromethyl–pyrazole–carboxamide derivatives as potential NSAID candidates, with a focus on achieving selective COX-2 inhibition and reduced cytotoxicity. In addition, their potential anticancer effects and pharmacokinetic properties were evaluated through in vitro and in silico analyses.

Methods The coupling reaction of aniline derivatives and pyrazole-carboxylic acid was used to synthesize a series of trifluoromethyl–pyrazole–carboxamide derivatives. Initially, the newly synthesized compounds were characterized using FTIR, HRMS, ^{1}H-NMR, ^{13}C-NMR, and MicroED techniques. Their inhibitory activities and potential selectivity against the key isoenzymes COX-1 and COX-2 were evaluated in vitro using a COX inhibition assay kit. Furthermore, the cytotoxicity of these compounds was assessed using an MTS assay against human normal cell lines (HEK293T) and hepatic cell lines (LX-2), as well as molecular docking and ADMET analyses were conducted.

Results Based on the biological evaluation, compound **3b** exhibited the most potent inhibitory activity against the COX-1 enzyme, with an IC_{50} value of 0.46 µM. Additionally, it demonstrated notable COX-2 inhibitory activity, with an IC_{50} value of 3.82 µM. In contrast, compound **3g** showed the highest selectivity ratio for COX-2 (1.68), alongside potent COX-2 inhibition (IC_{50} = 2.65 µM), outperforming the reference drug ketoprofen, which displayed a selectivity ratio of 0.21 and an IC_{50} value against COX-2 of 0.164 µM. Furthermore, compound **3d** exhibited strong COX-2 selectivity (selectivity ratio = 1.14) with an IC_{50} value of 4.92 µM. All synthesized compounds demonstrated negligible cytotoxic effects against the tested normal cell lines. However, compound **3a** exhibited cytotoxic activity against CaCo-2, MCF-7, Hep3B and HepG2 cancer cell lines with IC_{50} range 43.01–58.04 µM. Molecular docking studies revealed the

*Correspondence:
Mohammed Hawash
mohawash@najah.edu

Full list of author information is available at the end of the article

formation of favorable interaction profiles within the respective binding sites, which were comparable to those of the control agent ketoprofen, supporting the potent in vitro inhibitory activities observed. Pharmacokinetic analysis of the newly synthesized compounds indicated favorable properties regarding absorption, distribution, metabolism, excretion, and toxicity (ADMET), confirming the drug-like profiles of these chemical structures. Consequently, these agents are highly recommended for further investigation in clinical studies.

Conclusion Compounds 3b, 3d, and 3g demonstrated potent COX inhibition with notable COX-2 selectivity, supporting their promise as leads for safer anti-inflammatory drug development. Additionally, compound 3a displayed moderate cytotoxic effects against several cancer cell lines, suggesting possible dual anti-inflammatory and anticancer potential. Overall, the favorable drug-like properties and low toxicity profiles justify further preclinical investigation of these pyrazole–carboxamide derivatives.

Keywords COX, Anti-inflammatory agents, NSAIDs, Cytotoxicity, Trifluoromethyl-Pyrazole, MicroED

Background

A minimum of 2,500 years ago, Hippocrates recommended using willow bark extracts to treat fever and ease childbirth pain, marking the earliest recorded use of substances with analgesic, anti-inflammatory, and antipyretic effects. The formal history of nonsteroidal anti-inflammatory drugs (NSAIDs) began with the identification of salicin's pharmacological properties, followed by the discovery of salicylic acid and its synthetic derivative, acetylsalicylic acid (aspirin), which remains one of the most widely utilized over-the-counter medications [1]. A major milestone occurred in 1971, when the mechanism of NSAIDs was elucidated as the inhibition of prostaglandin synthesis via suppression of the cyclooxygenase (COX) pathway [2, 3].

Subsequent research revealed that cyclooxygenase enzymes, COX-1 and COX-2, share structural similarities but possess distinct biological roles. Detailed analysis of their amino acid sequences uncovered minimal yet crucial differences: for example, at positions 434 and 523, COX-1 contains isoleucine (Ile), whereas COX-2 substitutes valine (Val) at these positions. This substitution enlarges the COX-2 binding site by approximately 25% compared to COX-1, providing a critical foundation for designing bulky agents selective for COX-2 [4, 5]. Regarding physiological distribution, COX-1 is constitutively expressed in tissues such as the stomach and kidneys, playing a key role in maintaining gastric mucosal integrity and renal function. In contrast, COX-2 is typically inducible and upregulated during inflammation. Although non-selective NSAIDs effectively alleviate inflammation, they often produce gastrointestinal and renal side effects due to COX-1 inhibition. Recognizing the protective functions of COX-1 spurred the development of COX-2 selective inhibitors (coxibs) aimed at minimizing toxicity while preserving anti-inflammatory efficacy [6, 7]. Nevertheless, concerns regarding NSAID-associated toxicity have continued to drive the search for safer and more effective anti-inflammatory agents [8]. Current COX-2 inhibitors, such as celecoxib, while effective, have been associated with cardiovascular risks, prompting the development of novel scaffolds with improved selectivity and safety profiles [9].

Chemically, NSAIDs are diverse but generally classified based on their COX selectivity and structural characteristics. They are typically weak organic acids with hydrophobic properties, which facilitate their penetration into inflammatory sites and access to the hydrophobic channels within COX enzymes [10]. Among these, trifluoromethyl (-CF_3) substitutions are particularly valuable due to their ability to enhance metabolic stability, improve membrane permeability, and modulate binding affinity in drug-like molecules. Depending on their inhibitory potency ratio toward COX-1 and COX-2, NSAIDs are broadly categorized as either non-selective or COX-2 selective inhibitors [11].

Pyrazole-based heterocycles have gained significant interest in medicinal chemistry owing to their planar, electron-rich structures, which facilitate target-specific binding and versatile chemical modification. Within medicinal chemistry, heterocyclic compounds — characterized by ring structures containing atoms such as nitrogen, oxygen, or sulfur — serve as key scaffolds. Their incorporation enhances bioavailability, solubility, and pharmacological activity, contributing to a wide range of therapeutic effects including anti-inflammatory, analgesic, antimicrobial, anticancer, and antioxidant activities [12, 13]. Several established anti-inflammatory agents, such as indomethacin and piroxicam, incorporate heterocyclic frameworks.

Among heterocyclic systems, the pyrazole nucleus stands out for its versatility and biological significance. Pyrazole derivatives have demonstrated a wide range of pharmacological activities, including anti-cancer, anti-inflammatory, antiviral, and antibacterial properties [14, 15]. Notably, many COX-2 selective inhibitors, such as celecoxib and SC-558, incorporate a pyrazole scaffold, leveraging its planar, lipophilic structure to achieve potent bioactivity [10, 11]. This makes pyrazole chemistry

an attractive platform for designing and developing novel anti-inflammatory agents.

The dual role of COX-2 in both inflammation and oncogenesis makes it an attractive target not only for anti-inflammatory therapy but also for cancer chemoprevention. Beyond inflammation, the COX pathway has also been implicated in carcinogenesis, influencing critical processes such as angiogenesis, invasion, and apoptosis [16]. COX-2 is frequently overexpressed in various cancers, and inhibition of this pathway has shown potential in cancer prevention and therapy [17, 18]. Moreover, recent studies have highlighted the efficacy of NSAID-metal complexes in targeting cancer stem cells (CSCs), offering promising new strategies against aggressive tumors [19].

Preclinical studies further support the anti-cancer potential of COX inhibitors. Agents such as *mofezolac*, *nimesulide*, and *sulindac* have demonstrated significant tumor-suppressive effects in animal models, primarily through the modulation of apoptosis and angiogenesis pathways [20]. These findings underscore the pivotal role of prostaglandin biosynthesis and COX inhibition in regulating tumor growth and progression. Recent literature also highlights several pyrazole-based chemical structures exhibiting dual anti-inflammatory and anticancer activities (e.g., Compounds **St.1**–**St.6**, Fig. 1) [21–26], further reinforcing the therapeutic relevance of pyrazole scaffolds in oncology and inflammatory disease management.

To our knowledge, this is the first study to integrate MicroED crystallographic analysis, in vitro enzyme inhibition, cytotoxicity profiling, and computational modeling of trifluoromethyl-pyrazole–carboxamide derivatives in a single comprehensive framework. Building upon this background, the present study aims to design and synthesize a series of novel trifluoromethyl-pyrazole–carboxamide derivatives with potent inhibitory activity against COX-1 and COX-2, specifically targeting high COX-2/COX-1 selectivity profiles. The newly synthesized compounds will be structurally characterized and evaluated for their in vitro inhibitory activities against COX enzymes, with a primary focus on achieving COX-2 selectivity and reduced toxicity. In parallel, cytotoxicity assays will be performed on both normal and cancer cell lines to assess their anticancer potential. Computational docking studies will be undertaken to elucidate binding modes within the COX active sites, and pharmacokinetic profiling will be used to assess drug-likeness.

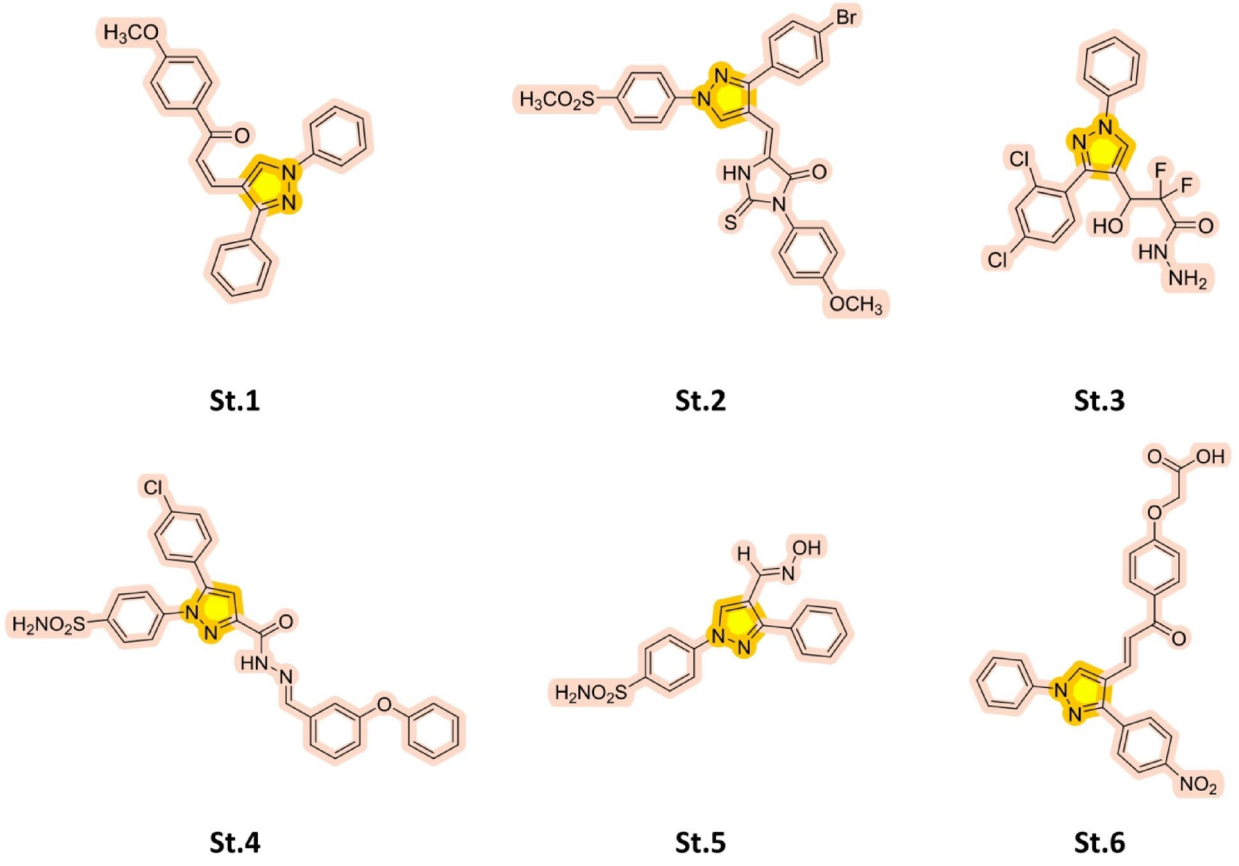

Fig. 1 Chemical structures of pyrazole-based agents exhibiting potential dual anti-inflammatory and anticancer activities

Methods

Reagents, materials and instruments

All chemicals were purchased from C.S. Chemicals Company, Alfa Aesar, and Sigma-Aldrich without any further purification. Additional equipment included a Vacuubrand rotary evaporator (complete set), RO UV lamp, LABOMED inverted fluorescence microscope, ESCO laminar flow cabinet, BIOBASE medical CO_2 incubator, Lab Tech digital water bath, J.P. SELECTA digital vortex, Memmert oven, and SHIMADZU analytical balance. ^{1}H- and ^{13}C-NMR spectra were obtained using a Bruker DPX-400 high-performance digital FT-NMR spectrometer, operating at 400 MHz for ^{1}H and 100 MHz for ^{13}C measurements. DMSO-d_6 was used as the solvent, and chemical shifts (δ) were reported in parts per million (ppm) relative to tetramethylsilane (TMS), with coupling constants (J values) expressed in Hertz (Hz). High-resolution mass spectra (HRMS) were recorded using a Waters LCT Premier XE mass spectrometer employing the ESI (+) ionization mode. Both NMR and HRMS analyses were performed at the Faculty of Pharmacy, Gazi University, Ankara, Turkey. The COX inhibitor screening assay kit No. 560,131 (Cayman Chemical, USA) was employed to evaluate the inhibitory activity against ovine COX-1 and human recombinant COX-2 enzymes. The enzymatic reaction was monitored by measuring the yellow chromophore product at 415 nm using a Bio-Rad UV-visible spectrophotometer equipped with a microplate reader.

MicroED: sample preparation, data collection, and refinement procedure

Following synthesis, compounds **3b**, **3d**, and **3h** were obtained as crystalline powders, eliminating the need for additional crystallization steps. A portion of each sample was manually ground using a mortar and pestle. For MicroED analysis, the powdered material was directly deposited onto glow-discharged lacey carbon-coated copper grids (200 mesh). Diffraction data acquisition was performed using a Thermo Fisher Scientific Glacios cryo-TEM, operating at 200 kV with the sample maintained at − 192 °C. The microscope featured a field emission electron source, a CETA-D camera (Thermo Fisher Scientific, Waltham, MA, USA), and an automated loading system capable of handling twelve grids simultaneously. Data collection was controlled via EPU-D software (v1.15). Instrument parameters included a 50 µm condenser aperture, spot size 11, and gun lens 8. Low-dose parallel illumination was employed to minimize beam damage. Crystals were continuously rotated between − 60 ° and + 60° in diffraction mode. Images were acquired in rolling shutter mode with 2× hardware binning and an exposure time of 0.5 s per frame. The resulting datasets were converted to SMV format, including necessary metadata for downstream crystallographic processing [20].

The unit-cell parameters determination, integration of the reflection intensities, and data reduction were performed using CrysAlis PRO software (Rigaku OD, 2025). The structures were solved in SHELXT [27] and refined using Olex2 [28] with the application of kinematical diffraction theory. After standard IAM refinement in olex2.refine, the TAAM refinement was applied using the MATTS data bank through the DiSCaMB utility program (discambMATTS2tsc.exe version 2.006) [29, 30], and the NoSpherA2 [31] module of Olex2. It was shown that TAAM refinement leads to better quality structural refinements than IAM [32]. Non-hydrogen atoms were refined with anisotropic displacement parameters, applying RIGU restraints to maintain reasonable thermal motion constraints. Hydrogen atom positions were generated computationally and refined using a riding model, with appropriate HFIX instructions to define their geometric parameters. For precision, X–H bond distances were fixed to standardized values derived from neutron diffraction studies, ensuring consistency with experimentally established geometries [33].

MicroED method

Compound **3b** crystallized in a triclinic system featuring a centrosymmetric space group, *P*-1, and the following lattice parameters: a = 9.1572(4) Å, b = 10.0658(5) Å, c = 12.0706(9) Å, and α = 87.064(5)°, β = 68.385(5)°, γ = 72.076(4)°. However, compound **3d** and **3h** were crystallized within the centrosymmetric space group of the monoclinic crystal system, $P2_1/c$, accompanied by the lattice parameters of a = 4.6946(7) Å, b = 16.9530(3) Å, c = 23.2720(4) Å, and β = 93.166(15)° and a = 15.4320(7) Å, b = 10.0856(19) Å, c = 13.4930(2) Å, and β = 94.770(3)°, respectively. All of the compounds have one molecule in their asymmetric unit. The R1 factors for compounds **3b**, **3d** and 3 h were recorded at 14.76%, 12.30% and 13.36%, respectively, consistent with typical results for kinematical refinement on **3d** ED data involving organic crystals.

General synthetic procedures

In a flame-dried round-bottom flask under an argon atmosphere, 4-dimethylaminopyridine (DMAP, 36.3 mg, 0.297 mmol) was added to a stirred solution of 1-(4-nitrophenyl)-5-(trifluoromethyl)-1*H*-pyrazole-4-carboxylic acid (300 mg, 0.99 mmol) in anhydrous dichloromethane (15 mL). Subsequently, 1-ethyl-3-(3-dimethylaminopropyl)carbodiimide hydrochloride (EDCI·HCl, 246.7 mg, 1.29 mmol) was introduced as the coupling agent, followed by the dropwise addition of the corresponding aniline derivative (1.1 equiv). The reaction mixture was stirred for 30 min at ambient temperature

and then allowed to proceed for 48–72 h under an inert atmosphere to avoid oxidative degradation [34].

Reaction progress was monitored via thin-layer chromatography (TLC), employing ninhydrin staining to detect residual amines and bromocresol green to assess the presence of unreacted carboxylic acid. Upon completion, the reaction mixture was transferred to a separatory funnel and washed with 32% hydrochloric acid to remove excess amine. The organic phase was dried over anhydrous Na_2SO_4, filtered, and concentrated under reduced pressure.

To facilitate purification, a small quantity of silica gel was added to the concentrated residue prior to solvent removal, considering the low boiling point of DCM (39.6 °C). The resulting silica-adsorbed crude was subjected to flash chromatography on silica gel using an appropriate gradient elution system. Fractions containing the desired product were pooled, evaporated, and dried under vacuum to afford the corresponding pyrazole–carboxamide derivatives as solids.

Synthesis of N-(4-(tertbutylphenyl)-1-(4-nitrophenyl)-5-(trifluoromethyl)-1H-pyrazole-4-carboxamide (3a)

The synthesis was carried out following the general procedure described above, using 4-tert-butylaniline (173.4 µL, 1.089 mmol) as the amine component. After completion of the reaction and workup, the crude product was adsorbed onto silica gel and purified by flash column chromatography using a 3:2 mixture of hexane and ethyl acetate as the eluent. The target compound was obtained as a beige solid (Rf = 0.66; solvent system: ethyl acetate/hexane = 2:3) in 88.6% yield. HRMS (m/z): [M + H] + Calc. for $C_{22}H_{20}F_3N_4O_3$, 433.1488 found 433.1487. ^{1}H-NMR (DMSO-d_6, 500 MHz) δ ppm: 10.56 (s, 1H), 8.54–8.48 (m, 2 H), 8.46 (s, 1H), 7.97–7.90 (m, 2 H), 7.71–7.64 (m, 2 H), 7.47–7.41 (m, 2 H), 1.33 (s, 9 H). ^{13}C-NMR (DMSO-d6, 125 MHz) δ ppm: 158.87, 148.39, 146.94, 143.83, 141.21, 136.50, 130.60, 130.29, 127.67, 125.90, 125.41, 123.02, 122.91, 120.76, 120.09, 118.61, 34.57, 31.65, 1.57.

Synthesis of N-(4-chloro-2,5-dimethoxyphenyl)-1-(4-nitrophenyl)-5-(triflouromethyl)-1H-pyrazole-4-carboxamide (3b)

Following the general synthetic procedure, 4-chloro-2,5-dimethoxyaniline (204.3 mg, 1.089 mmol) was employed as the aniline coupling partner. Upon completion of the reaction and standard aqueous workup, the crude product was pre-adsorbed onto silica gel and purified by flash column chromatography using hexane/ethyl acetate (3:2, v/v) as the eluent. The target compound was isolated as a yellow solid with an Rf value of 0.60 (solvent system: ethyl acetate/hexane = 2:3), affording a yield of 89%. HRMS (m/z): [M + H] + Calc. for $C_{19}H_{14}ClF_3N_4O_5$, 471.0683 found 471.0684. ^{1}H NMR (400 MHz, DMSO) δ 9.88 (s, 1H), 8.50–8.44 (m, 2 H), 7.94–7.84 (m, 2 H), 7.77 (s, 1H), 7.30–7.20 (m, 1H), 3.83 (s, 6 H). ^{13}C-NMR (101 MHz, DMSO) δ: 159.34, 148.57, 148.39, 145.54, 143.88, 141.33, 127.70, 126.50, 125.38, 122.51, 121.00, 118.31, 117.30, 114.12, 108.97, 57.12, 56.97.

Synthesis of N-(3,5-dimethoxyphenyl)-1-(4-nitrophenyl)-5-(trifluoromethyl)-1H-pyrazole-4-carboxamide (3c)

According to the general procedure, 3,5-dimethoxyaniline (166.8 mg, 1.089 mmol) was used as the aniline component. After completion of the reaction and standard aqueous extraction, the crude residue was adsorbed onto silica gel and subjected to column chromatography using hexane/ethyl acetate (3:2, v/v) as the mobile phase. The product was obtained as a pale-yellow solid with an Rf value of 0.43 (solvent system: ethyl acetate/hexane = 2:3), yielding 85.3%. HRMS (m/z): $[M + H]^+$ calc. For $C_{19}H_{15}F_3N_4O_5$, 437.1073 found 437.1076. ^{1}H NMR (400 MHz, DMSO) δ: 10.50 (s, 1H), 8.50–8.39 (m, 3 H), 7.96–7.83 (m, 2 H), 6.99 (d, *J* = 2.2 Hz, 2 H), 6.32 (s, 1H), 3.76 (s, 6 H). ^{13}C-NMR (101 MHz, DMSO) δ: 161.00, 159.09, 148.42, 143.79, 141.25, 140.72, 127.69, 125.41, 122.88, 120.99, 118.31, 98.59, 96.54, 55.65.

Synthesis of N-(3,4-dimethoxyphenyl)-1-(4-nitrophenyl)-5-(triflouromethyl)-1H-pyrazole-4-carboxamide (compound 3d)

Following the general synthetic procedure, 3,4-dimethoxyaniline (166.8 mg, 1.089 mmol) was employed as the aniline derivative. Upon completion of the reaction and aqueous workup, the crude residue was pre-adsorbed onto silica gel and purified by column chromatography using a 1:1 mixture of dichloromethane and ethyl acetate as the eluent. The product was isolated as a fine beige solid with an Rf value of 0.71 (solvent system: DCM/ethyl acetate = 1:1), yielding 55.4%. HRMS (m/z): [M + H] + calcd. For $C_{19}H_{15}F_3N_4O_5$, 437.1073 found 437.1076. ^{1}H-NMR (400 MHz, DMSO) δ: 10.38 (s, 1H), 8.51–8.43 (m, 2 H), 8.41 (s, 1H), 7.94–7.82 (m, 2 H), 7.40 (d, J = 2.4 Hz, 1H), 7.26 (d, J = 8.6, 2.4 Hz, 1H), 6.96 (d, J = 8.7 Hz, 1H), 3.77 (d, J = 5.3 Hz, 6 H). ^{13}C-NMR (101 MHz, DMSO) δ 158.59, 149.03, 148.40, 145.92, 143.85, 141.22, 132.62, 127.68, 125.40, 123.06, 121.04, 118.35, 112.48, 112.36, 105.36, 56.21, 55.91.

Synthesis of N-(4-(methylthio)phenyl)-1-(4-nitrophenyl)-5-(triflouromethyl)-1H-pyrazole-4-carboxamide (compound 3e)

In accordance with the general procedure, photosensitive 4-(methylthio)aniline (135.5 µL, 1.089 mmol) was used as the aniline derivative. After completion of the reaction and standard workup, the crude residue was adsorbed onto silica gel and purified via flash column chromatography using hexane/ethyl acetate (3:2, v/v) as the eluent.

The final product was obtained as a soft white solid with an Rf value of 0.53 (solvent system: ethyl acetate/hexane = 2:3), in 92.4% yield. HRMS (m/z): $[M+H]^+$ calcd. For $C_{18}H_{13}F_3N_4O_3S$, 423.0739 found 423.0733. ^{1}H-NMR (400 MHz, DMSO) δ: 10.58 (s, 1H), 8.53–8.39 (m, 3 H), 7.93–7.87 (m, 2 H), 7.69 (d, J = 8.8 Hz, 2 H), 7.34–7.28 (m, 2 H), 2.49 (s, 3 H). ^{13}C-NMR (101 MHz, DMSO) δ: 158.91, 148.42, 144.62, 143.81, 141.25, 136.47, 133.42, 130.72, 130.56, 130.33, 127.70, 127.43, 125.40, 120.98, 116.20, 115.82, 15.85.

Synthesis of N-([1,1′-biphenyl]-4-yl)-1-(4-nitrophenyl)-5-(trifluoromethyl)-1H-pyrazole-4-carboxamide (compound 3f)

Following the general procedure, 4-aminobiphenyl (184.3 mg, 1.089 mmol) was used as the aniline component. After completion of the reaction and aqueous workup, the crude product was adsorbed onto silica gel and subjected to column chromatography using a 4.5:0.5 mixture of dichloromethane and methanol as the mobile phase. The desired product was obtained as a white crystalline solid with an Rf value of 0.90 (solvent system: DCM/methanol = 4.5:0.5), affording a yield of 53.1%. HRMS (m/z): $[M+H]^+$ calcd. For $C_{23}H_{15}F_3N_4O_3$, 453.1175 found 453.1177. ^{1}H-NMR (400 MHz, DMSO) δ 10.69 (s, 1H), 8.52–8.43 (m, 3 H), 7.91 (d, J = 8.6 Hz, 2 H), 7.83 (d, J = 8.4 Hz, 2 H), 7.75–7.66 (m, 4 H), 7.53–7.45 (m, 2 H), 7.40–7.33 (m, 1H). ^{13}C-NMR (101 MHz, DMSO) δ 159.08, 148.43, 143.81, 141.28, 140.06, 138.54, 136.22, 130.75, 129.41, 127.72, 127.67, 127.49, 126.82, 125.42, 122.90, 121.03, 120.68, 118.34.

Synthesis of N-(4-(2-methoxyphenyl)phenyl)-1-(4-nitrophenyl)-5-(trifluoromethyl)-1H-pyrazole-4-carboxamide (compound 3 g)

In accordance with the general procedure, 4-(2-methoxyphenyl)aniline (234.4 mg, 1.089 mmol) was used as the aniline derivative. Following completion of the reaction and aqueous workup, the crude product was adsorbed onto silica gel and purified by column chromatography using a 1:1 mixture of dichloromethane and ethyl acetate as the eluent. The target compound was obtained as a fine white powder with an Rf value of 0.83 (solvent system: DCM/ethyl acetate = 1:1), affording a yield of 54.8%. HRMS (m/z): [M + H] + calcd. For $C_{24}H_{17}F_3N_4O_5$, 499.1229 found 499.1228. ^{1}H-NMR (400 MHz, DMSO) δ: 10.52 (s, 1H), 8.50–8.40 (m, 3 H), 7.93–7.85 (m, 2 H), 7.69–7.59 (m, 2 H), 7.24–7.16 (m, 2 H), 7.07–6.95 (m, 2 H), 6.92–6.84 (m, 2 H), 3.77 (s, 3 H). ^{13}C-NMR (101 MHz, DMSO) δ: 158.75, 154.50, 151.69, 148.40, 144.47, 143.83, 141.23, 133.63, 130.28, 127.69, 125.81, 125.40, 122.95, 121.98, 121.88, 121.65, 121.56, 121.03, 118.34, 117.05, 113.90, 56.10.

Synthesis of 1-(4-nitrophenyl)-5-(trifluoromethyl)-N-(3,4,5-trimethoxyphenyl)-1H-pyrazole-4-carboxamide (compound 3 h)

Following the general synthetic procedure, 3,4,5-trimethoxyaniline (199.5 mg, 1.089 mmol) was used as the aniline coupling partner. Upon completion of the reaction and standard aqueous workup, the crude product was adsorbed onto silica gel and purified by gravity column chromatography using a 1:1 mixture of dichloromethane and ethyl acetate as the eluent. The desired compound was obtained as a pale-yellow fine powder with an Rf value of 0.63 (solvent system: DCM/ethyl acetate = 1:1), affording a yield of 61.6%. HRMS (m/z): [M + H] + calcd. For $C_{20}H_{17}F_3N_4O_6$, 467.1178 found 467.1176. ^{1}H-NMR (400 MHz, DMSO) δ: 10.48 (s, 1H), 8.53–8.38 (m, 3 H), 7.96–7.83 (m, 2 H), 7.13 (d, J = 1.4 Hz, 2 H), 3.79 (d, J = 1.4 Hz, 6 H), 3.66 (d, J = 1.4 Hz, 3 H). ^{13}C-NMR (101 MHz, DMSO) δ 158.84, 153.24, 148.42, 143.82, 141.24, 135.23, 134.50, 130.74, 130.35, 127.69, 125.40, 122.90, 121.01, 118.32, 98.02, 60.62, 56.25.

Cell culture and cytotoxicity assay

To support the growth of human hepatic stellate (LX-2) cells and HEK293T cells, RPMI-1640 medium was supplemented with 1% L-glutamine, 10% fetal bovine serum (FBS), and antibiotics (penicillin and streptomycin). During medium changes, the culture flasks were gently tilted to carefully remove the spent medium without disrupting the cell monolayer. Similarly, Dulbecco's Phosphate-Buffered Saline (DPBS) was carefully aspirated to avoid damaging the cells. Following this, 1 mL of trypsin–EDTA solution was added to the culture flask and gently rotated before incubation at 37 °C for 5 min. Once the majority of the cells had detached, 10 mL of complete growth medium was added to neutralize the trypsin. The culture suspension was gently mixed or pipetted to ensure complete neutralization. After 24 h, the medium was carefully replaced to minimize disturbance of the cell layer. Different concentrations of the test compounds were added to each well in 100 µL increments, followed by incubation at 37 °C for 72 h without disturbing the cells. To assess cell viability, the CellTiter 96® AQueous One Solution Cell Proliferation (MTS) Assay (Promega Corporation, Madison, WI, USA) was performed according to the manufacturer's instructions. After adding 20 µL of MTS reagent to each well, plates were incubated for 2 h at 37 °C. Absorbance was measured at 490 nm using an ELISA plate reader to determine cell viability and calculate IC_{50} values. The remaining reagents and plates were stored at − 20 °C [20].

Biological assay on COX enzyme screening kits

This study assessed the inhibitory effects of the synthesized compounds on human recombinant COX-2 and

bovine COX-1 using the COX (Human) Inhibitor Screening Assay Kit (Cayman Chemical, Cat. No. 560131). Due to their structural resemblance to celecoxib, the prepared products were compared against celecoxib, which served as the positive control. All reagents were prepared, and assay procedures were performed following the manufacturer's instructions. The test compounds were dissolved in dimethyl sulfoxide (DMSO) at two concentrations (40 µM and 10 µM). Celecoxib was similarly prepared as a reference. Subsequently, COX-1 or COX-2 enzymes were incubated with the inhibitors for 10 min at 37 °C in a diluted reaction buffer. The reaction was initiated by the addition of 10 µL of arachidonic acid, followed by incubation at 37 °C for 30 s. To terminate the enzymatic reaction, 30 µL of stannous chloride solution was added, and the mixture was allowed to sit at room temperature for 5 min. The resulting prostaglandin levels were quantified by ELISA. After loading the samples, the 96-well plates were sealed with plastic film and incubated on an orbital shaker at room temperature for 18 h. Plates were then washed five times with wash buffer, and each well received 200 µL of Ellman's reagent along with 5 µL of tracer solution, except for the total activity (TA) wells [20].

The plate was incubated in the dark at room temperature for 60 to 90 min, or until the absorbance of the B_0 wells reached between 0.3 and 0.8 at 405 nm. Absorbance was measured using a Microplate Reader 6000 Unilab. Inhibitory curves were generated to calculate the IC_{50} values for COX-1 and COX-2. Finally, the selectivity index (SI) was determined by dividing the IC_{50} value of COX-1 by that of COX-2 [20].

Computational studies

The use of computers has proven to be a highly advantageous tool, offering precision and speed across various aspects of life. Over the past decades, computer-aided drug design and development have emerged as valuable investments and essential strategies for discovering new pharmacologically active agents. Among these techniques, molecular docking studies are considered one of the most trusted tools for predicting biological activity and, in many cases, the binding affinity of small molecules with high accuracy. Molecular docking aims to visualize the pose of ligands within the binding domain of target proteins, providing a comprehensive picture of occupied space, involved physical forces, environmental setting, and the nature of surrounding residues. Consequently, this technique can help explain observed in vitro results and offer valuable insights to enhance the activity profiles of therapeutic agents [35].

Protein Preparation: molecular docking studies began with the selection of crystallographic structures of the target proteins. For the cyclooxygenase I (COX-1) enzyme, the X-ray crystal structure with PDB ID: 3KK6 (resolution: 2.75 Å, R-value observed: 0.208) was selected. For the cyclooxygenase II (COX-2) enzyme, the crystallographic structure with PDB ID: 5KIR (resolution: 2.70 Å, R-value observed: 0.180) was chosen. Both protein crystal structures had been previously optimized and validated in our earlier studies, confirming their high suitability and reliability for producing precise and reproducible docking results [36–38]. Importantly, the Ovis aries COX-1 shares a high degree of conservation with the human COX-1 enzyme, particularly in the catalytic binding site residues essential for ligand recognition and activity. The active site residues such as Arg120, Tyr355, Ser530, Tyr385, etc., are structurally conserved between Ovis aries and human COX-1 (as inferred from sequence alignments and previous structural comparisons using PDB entries) [39]. For example, PDB entry 6Y3C is a human COX-1 structure (Homo sapiens) with resolution ~ 3.36 Å, which confirms similar spatial arrangement of the active site portion [4]. Also, in the absence of a higher-resolution human COX-1 crystal structure that fully captures the active site, the Ovis aries structure 3KK6 serves as a valid and widely accepted surrogate for docking studies. Its use enables reliable comparisons and predictions of inhibitor binding that are expected to translate well to the human enzyme [40, 41]. The selected protein structures were modeled, refined, minimized, and optimized using default parameters through the Protein Preparation Wizard integrated into Maestro (Schrödinger Suite). These steps aimed to refine incomplete or terminal amide groups, correct topological states, assign missing hydrogen atoms, formal charges, and bond orders. Subsequently, water molecules located within 3 Å of any heteroatoms were deleted, and the ionization states were adjusted to simulate a physiological pH of 7.0 ± 2.0, ensuring the accuracy of the docking results. The orientations of retained water molecules were corrected, and intramolecular hydrogen bonds were properly assigned. Finally, to minimize steric clashes and reorient hydroxyl side chains, the refined structures were energy-minimized using the OPLS-2005 force field.

Receptor Grid Generation: following the preparation of the extracted protein crystallographic structures, a receptor grid was generated. Since the selected proteins were obtained in their holo forms (complexed with crystallographic ligands), these native ligands were utilized to define the binding sites. The receptor grids were then constructed by setting the grid box dimensions to 20 Å × 20 Å × 20 Å, centered on the position of the co-crystallized ligands.

Ligands Preparation: the chemical structures of the synthesized agents were initially generated using ChemDraw in CDX format, followed by extracting their SMILES strings and subjecting them to the LigPrep

module integrated into Maestro (Schrödinger Suite). Subsequently, **3d** configurations for each structure were generated, incorporating their ionization states at physiological pH (using the Epik module), as well as possible tautomeric and stereochemical variations. This step also aimed to correct bond orders, refine chiral centers, and address any missing structural elements to optimize and minimize the molecules. Finally, the chemical structures were further optimized using the Impact package (Schrödinger) under the OPLS-2005 force field, with minimization proceeding until reaching a convergence threshold of 0.001 Å RMSD. The fully prepared ligands were then saved for use in the docking studies.

XP-Glide Ligand Docking and Binding Free Energy: using the previously prepared chemical structures of the ligands and the receptor grids, extra precision (XP) Glide docking in flexible mode was performed. Docking scores and binding poses for each ligand within its respective binding site were recorded. To obtain more accurate binding profiles and estimate the free energy of binding, the docked complexes were further subjected to the Prime Molecular Mechanics Generalized Born Surface Area (Prime MM-GBSA) model, integrated within the Maestro Schrödinger suite, and the corresponding ΔG values were recorded. The procedure and parameters previously applied in our earlier studies [37]. The top-ranked ligand–protein complexes were then extracted as PDB files and subjected to analysis using the free Protein–Ligand Interaction Profiler (PLIP) server. This analysis provided a thorough evaluation of each complex, predicting the key physical interactions and measuring the binding distances between the ligands and their corresponding binding sites [42, 43]. Although Schrödinger's Maestro suite includes a Ligand Interaction Diagram module, PLIP was additionally employed because it offers an automated, standardized, and publication-validated platform that ensures reproducibility and facilitates independent verification of interaction patterns across different docking environments. Furthermore, PLIP's open-access nature allows cross-validation of the Schrödinger results while providing highly detailed interaction profiling (hydrogen bonds, hydrophobic contacts, π–π stacking, salt bridges, halogen bonds) with precise geometric parameters, thereby enhancing the robustness and transparency of the analysis [44, 45].

ADMET Analysis: the in silico pharmacokinetic profiles of the synthesized chemical structures were evaluated using the QikProp module integrated into the Maestro Schrödinger 14.2 suite.

Results and discussion

Chemistry

In line with rational drug design principles, the synthesis focused on introducing diverse electronic and steric substituents to modulate COX-2 selectivity and optimize drug-like behavior. Scheme 1 outlines the synthetic steps involved in the preparation and characterization of pyrazole–carboxamide derivatives from pyrazole acid and various substituted aniline derivatives. The starting materials include the pyrazole acid (referred to as "acid") and the aniline derivatives, bearing different substituents (R groups such as $-C_4H_9$, –Cl, and $-OCH_3$), which significantly influence the properties of the final products (e.g., compounds **3a**, **3b**, etc.). The pyrazole acid core was selected due to its proven bioisosteric utility in anti-inflammatory scaffolds and its potential to enhance π–π interactions and hydrophobic contacts within the COX active sites. The reactions were conducted in dichloromethane (DCM) under stirring for 48–72 h.

The use of EDCI as a coupling agent in combination with DMAP was preferred for its efficiency under mild conditions, minimizing by-product formation and

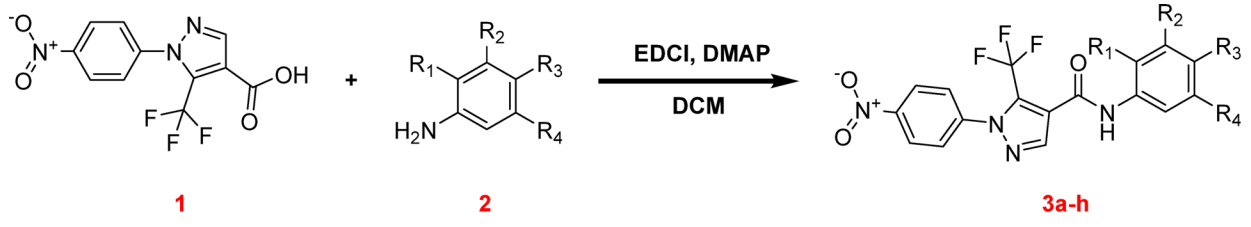

a: R_1, R_2=H, R_3= t-butyl
b: R_1= OCH_3, R_2=H, R_3= Cl, R_4= OCH_3
c: R_1, R_3 = H, R_2= OCH_3, R_4= OCH_3
d: R_1, R_2= H, R_3= OCH_3, R_4= OCH_3
e: R_1, R_2, R_4= H, R_3= SCH_3
f: R_1, R_2, R_4= H, R_3= phenyl
g: R_1, R_2, R_4= H, R_3= 2-methoxy phenoxy
h: R_1= H, R_2= OCH_3, R_3= OCH_3, R_4= OCH_3

Scheme 1 Synthesis of pyrazole-carboxamide derivatives (**3a**-h), stirring 72 h under inert gas

preserving the functional integrity of both aromatic and heterocyclic moieties. In the subsequent step, 4-dimethylaminopyridine (DMAP) and 1-ethyl-3-(3-dimethylaminopropyl) carbodiimide (EDCI) were introduced under an inert argon atmosphere to facilitate the acylation reaction. The successful formation of the targeted derivatives was confirmed by high-resolution mass spectrometry (HRMS), in which the experimentally observed masses closely matched the calculated values, validating the practical success of the synthetic approach.

The structures of the synthesized compounds were further elucidated using proton nuclear magnetic resonance (1 H NMR) spectroscopy. A characteristic amide proton signal appeared as a single peak within the range of 10.38–10.69 ppm, indicating successful acylation. Complex patterns observed in the aromatic region reflected the diverse substitutions on the aniline moiety. Signals attributed to the pyrazole ring were evident between 6.32 and 7.50 ppm, while the methoxy groups gave a distinct singlet around 3.77 ppm, further confirming the integrity of the pyrazole core. These characteristic shifts not only confirm the integrity of the target framework but also provide critical structural evidence supporting the success of the regioselective acylation strategy.

Additional structural insights were obtained from carbon-13 nuclear magnetic resonance (^{13}C-NMR) spectroscopy. A strong peak around 170 ppm was assigned to the carbonyl carbon of the amide group, affirming the formation of the carboxamide linkage. The aromatic carbons displayed multiple signals in the range of 90–160 ppm, consistent with the presence of complex aromatic frameworks. Such combined NMR analysis is crucial in establishing structure–activity relationships (SAR) and verifying the electronic influence of various R-groups on the pyrazole core.

Overall, the synthetic pathway successfully led to the generation of various aniline-derived pyrazole–carboxamide compounds. Characterization by HRMS, ^{1}H NMR, and ^{13}C-NMR strongly supports the structural integrity and successful formation of the designed derivatives. This detailed description not only verifies the chemical properties of the newly synthesized agents but also underscores the important spectroscopic features crucial for future applications. The introduction of diverse aniline-based substituents was designed to explore electronic and steric effects on COX inhibition, setting the stage for SAR analysis.

MicroED structural analysis

The key compounds in this study were analyzed using Microcrystal Electron Diffraction (MicroED), a specialized **3d** electron diffraction (**3d** ED) technique. This technique provides an advanced solution for pharmaceutical compounds that fail to yield high-quality single crystals for traditional X-ray diffraction, yet require atomic-resolution validation during early-stage drug discovery. MicroED is particularly useful for characterizing small molecules when sample quantities are limited or when traditional crystallization proves difficult, such as cases where only microcrystals form. It is particularly valuable in medicinal chemistry, where synthetic yields may be low and rapid structural confirmation is essential for guiding structure–activity relationship (SAR) studies. This method serves as a robust alternative to single-crystal X-ray diffraction (SCXRD), enabling atomic-level structural determination even for challenging samples via transmission electron microscopy (TEM). The growing application of MicroED in the pharmaceutical sciences highlights its role in the rapid structural characterization of novel heterocyclic drug candidates, such as pyrazole-based scaffolds. In this work, MicroED was employed because the compounds failed to produce crystals of sufficient size for conventional X-ray diffraction (XRD) analysis.

Microcrystals of compounds **3b**, **3d**, and **3h** were individually analyzed by electron diffraction (Figure S1), yielding complete datasets of satisfactory quality (Table S1). These compounds were selected based on their biological activity profiles and representative substitution patterns, providing insight into structure–conformation relationships. The structural refinement process employed a kinematical approximation, with anisotropic displacement parameters (ADPs) being refined for all non-hydrogen atoms in each compound. This enabled the confirmation of key geometrical features, such as the orientation of electron-donating and halogen substituents, which are hypothesized to affect binding affinity and COX isoform selectivity. After the refinement, all the ADPs of non-H atoms were positively defined, though for some, the Hirshfeld Difference was not acceptable. Therefore, the RIGU restrainers were used (Fig. 2). MicroED analysis successfully verified both the molecular composition and atomic connectivity of the synthesized compounds. This technique additionally enabled the first elucidation of their three-dimensional structures, representing previously unreported spatial configurations to the best of our knowledge. The structural overlay of compounds **3b**, **3d**, and **3h** with respect to the atoms N4-C11-O3 shows that the conformation of these compounds is different, as shown in Fig. 3. These conformational differences may influence ligand–protein interaction profiles, particularly within the flexible side pocket of COX-2. The crystallographic data and refinement parameters are summarized in Table S1. Collectively, MicroED provided rapid and reliable structural confirmation of selected bioactive compounds, reinforcing their suitability for further biological evaluation and SAR analysis.

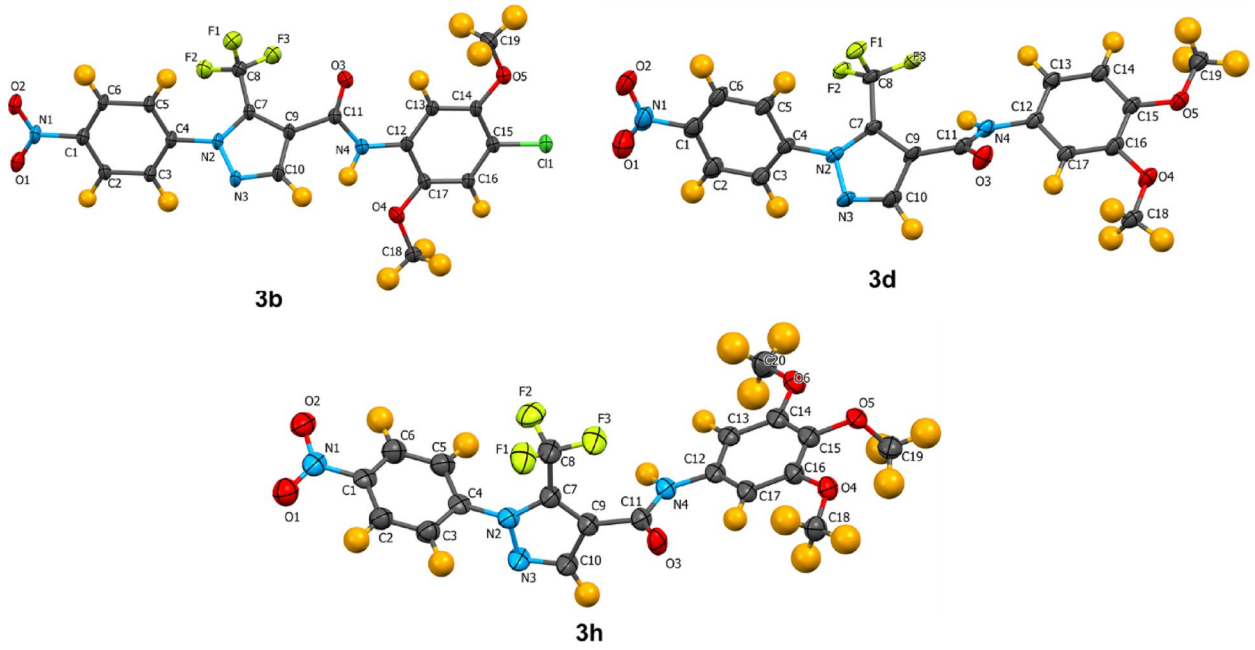

Fig. 2 Thermal ellipsoid views with a 50% probability level for all crystal structures with the labels of atoms

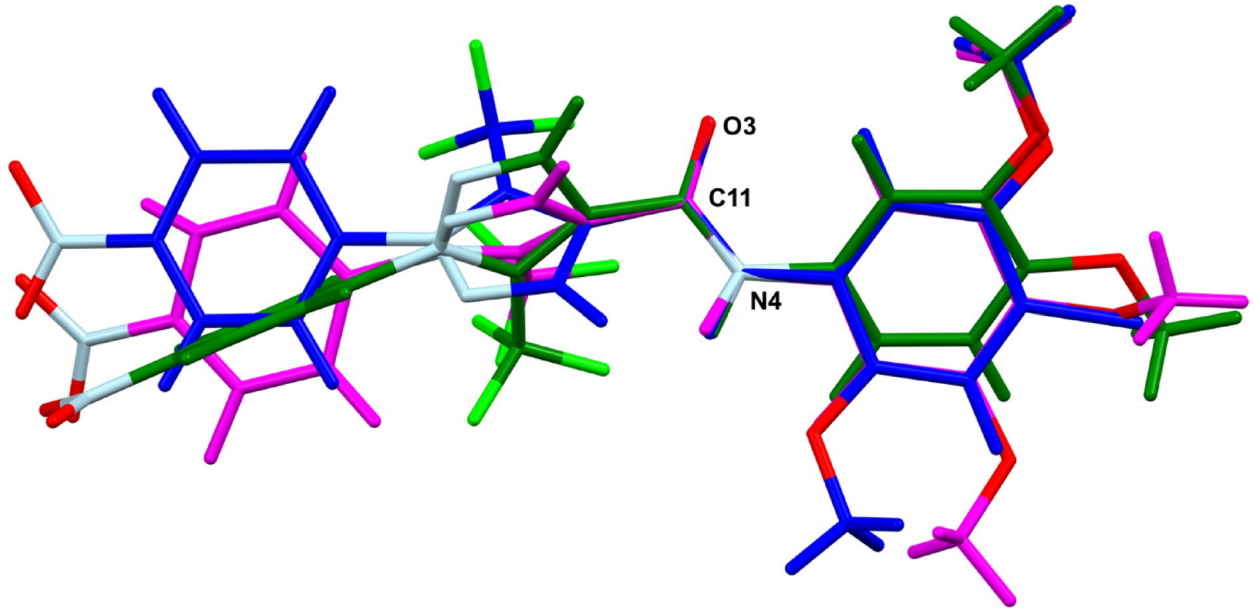

Fig. 3 Structure overlay diagrams of the compound **3a** (blue), **3d** (green) and 3 h (magenta)

COX inhibition and selectivity profiling

To evaluate the anti-inflammatory potential and isoform selectivity of the synthesized pyrazole–carboxamides, in vitro COX inhibition assays were conducted using human recombinant COX-2 and ovine COX-1 isoenzymes. Trifluoromethyl-pyrazole derivatives were known for its strong role as a selective inhibitor of COX-2 enzyme, which is implicated in inflammatory processes, these derivatives were characterized by its unique molecular feature (CF_3), that has garnered attention for its potential as a nonsteroidal anti-inflammatory drug (NSAID) that minimizes gastrointestinal side effects typically associated with nonselective COX inhibitors [46, 47]. The mechanism of these scaffolds involves a steric hindrance introduced by the CF3 group, which interferes with the binding interactions of substrates to the COX enzymes, thereby selectively inhibiting COX-2 while not fitting well with the COX-1 isoenzyme [48, 49]. Furthermore, the biological or pharmacological properties of this family of compounds indicate their diverse therapeutic

effects, which extend beyond pain reducing or relieving to include immune modulation and/or potential anticancer applications, accordingly to [50, 51].

Our results indicate that compound **3a** (bearing a 4-tert-butyl substituent) and compound **3e** (bearing a 4-methylthio substituent) exhibited similar inhibitory profiles, with relatively low potency against both COX-1 and COX-2. Their IC_{50} values were 6.62 ± 0.87 µM and 6.67 ± 1.81 µM for COX-1, and 9.03 ± 0.66 µM and 8.98 ± 1.85 µM for COX-2, respectively. However, both compounds demonstrated favorable selectivity indices when compared to the reference drug, ketoprofen, which was utilized as a positive control. Table 1 summarizes the calculated half-maximal inhibitory concentrations (IC_{50}) and selectivity indices (SI) for the synthesized trifluoromethyl–pyrazole–carboxamide derivatives, and the cytotoxicity results against normal cell lines. The presence of the trifluoromethyl group on the pyrazole scaffold likely contributed to enhanced lipophilicity and selective binding within the COX-2 hydrophobic side pocket, favoring isoform discrimination.

Ketoprofen, a widely used non-selective NSAID, served as the reference compound to validate the assay performance and benchmark compound selectivity. The introduction of a chloro atom in compound **3b** (bearing a chloro–dimethoxy moiety) substantially enhanced its inhibitory potency against COX-1, achieving approximately a fourfold improvement over compound **3c** and a tenfold improvement over compound **3d**, which possess only dimethoxy groups. Against COX-2, compound **3b** also exhibited slightly superior activity compared to **3c** and **3d**, with IC_{50} values of 3.82 ± 1.36 µM, 5.78 ± 0.47 µM, and 4.94 ± 2.29 µM, respectively. Among this subgroup, however, compound **3d** demonstrated the highest selectivity index (SI = 1.14).

Regarding COX-2 selectivity across all derivatives, compound **3g** exhibited the highest selectivity index (SI = 1.68), even higher than that of ketoprofen (SI = 0.21). The high selectivity index (SI = 1.68) observed for compound **3g** underscores its potential as a selective COX-2 inhibitor, a key criterion for minimizing COX-1-associated gastrointestinal toxicity. This marked selectivity is attributed to the presence of the bulky 2-methoxyphenoxy group, which favors binding within the COX-2 side pocket. Moreover, compound **3g** displayed the most potent COX-2 inhibitory activity among the synthesized compounds, with an IC_{50} value of 2.65 ± 1.55 µM.

Compounds **3f** and **3 h** also displayed favorable selectivity indices (0.98 and 0.93, respectively), suggesting that the introduction of a 4-aminobiphenyl group or trimethoxy substitution enhances COX-2 selectivity compared to ketoprofen. Collectively, the data support the identification of structurally optimized pyrazole–carboxamides with improved COX-2 selectivity profiles and minimal cytotoxicity against normal cell lines, thereby validating their potential as safe anti-inflammatory leads.

Evaluation of cytotoxicity (MTS-based cytotoxic evaluation of pyrazole-carboxamides)

Cytotoxicity (normal cell lines)

To assess the safety profile of the synthesized trifluoropyrazole–carboxamide derivatives, in vitro cytotoxicity assays were performed using MTS methodology on human kidney (HEK293T) and hepatic stellate (LX-2) cell lines. The assay was performed at five different concentrations (300, 100, 50, 10, and 1 µM). Test concentrations extended up to 300 µM to capture any off-target toxicity at supra-pharmacological levels, ensuring relevance to potential therapeutic index calculations. Despite the fact that the concentrations used for cytotoxicity testing were

Table 1 Shows IC_{50} values µM and selectivity (SI) for the synthesized derivatives against COX enzymes, and the Inhibition percentage at normal cell lines (LX-2 and Hek293t)

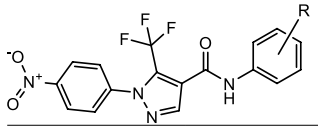

Code	R	IC_{50} µM		SI	% of inh. at 50 µM	
		COX1	COX2		LX-2	Hek293t
3a	4-tert-butyl	6.62 ± 0.87	9.03 ± 0.66	0.73	14.51 ± 1.55	19.73 ± 2.75
3b	4-chloro-2,5dimethoxy	0.46 ± 0.25	3.82 ± 1.36	0.12	2.08 ± 0.25	20.14 ± 1.65
3c	3,5-dimethoxy	1.74 ± 1.02	5.78 ± 0.47	0.3	14.05 ± 2.88	7.79 ± 0.81
3d	3,4-dimethoxy	5.59 ± 2.14	4.92 ± 2.29	1.14	4.78 ± 1.04	7.40 ± 0.69
3e	4-S-CH_3	6.67 ± 1.81	8.98 ± 1.85	0.74	11.25 ± 0.99	13.08 ± 1.08
3f	4-aminobiphenyl	5.91 ± 1.11	6.00 ± 1.33	0.98	12.42 ± 1.25	13.29 ± 2.00
3 g	4-(2-methoxyphenoxy)	4.45 ± 2.07	2.65 ± 1.55	1.68	9.97 ± 2.04	11.97 ± 1.68
3 h	3,4,5-trimethoxy	4.51 ± 0.45	4.82 ± 0.99	0.93	10.99 ± 0.15	10.60 ± 1.89
+ ve control		0.035 ± 0.01[a]	0.164 ± 0.12[a]	0.21[a]	81.36 ± 2.42[b]	73.05 ± 2.35[b]

[a] ketoprofen, [b] 5-FU, p Value < 0.05

tenfold higher than those used for COX enzyme inhibition assays, all compounds exhibited low inhibition percentages on HEK293T cells compared to the reference drug 5-fluorouracil (5-FU). The detailed inhibition profiles are illustrated in Fig. 4.

All synthesized compounds displayed minimal cytotoxic effects against the evaluated normal cell lines, with cell viability percentages remaining close to the levels observed in the DMSO control group (vehicle control without active drug). This finding is of particular interest for NSAID development, where systemic exposure often leads to gastrointestinal and renal toxicity due to off-target effects. Moreover, cytotoxicity testing of the trifluoromethyl–pyrazole–carboxamide derivatives against LX-2 cells at 50 µM (Fig. 5) revealed a similarly favorable safety profile, further confirming the non-toxic nature of these compounds. Overall, the low toxicity against non-cancerous cell lines supports the safety and drug-likeness of these pyrazole-based agents, reinforcing their candidacy for further in vivo investigation. The full cytotoxicity results for all tested compounds, compared to the positive control 5-FU, are presented in Fig. 5.

Anticancer activity (cancer cell lines)

The anticancer activity of the newly developed trifluoromethyl–pyrazole–carboxamide derivatives was evaluated against various cancer cell lines, as shown in Fig. 5. Most compounds exhibited low anticancer activity; however, compound 3a was an exception. At 50 µM concentration, compound 3a reduced the viability of CaCo-2, HepG2, and Hep3B cells to approximately 50%, suggesting selective cytotoxicity toward tumor cells. Its IC_{50} values ranged from 43.01 to 58.04 µM against CaCo-2, HepG2, HeLa, MCF-7, and Hep3B cell lines. The dose-dependent inhibition patterns are illustrated in Fig. 6. The selective cytotoxicity of compound **3a**, particularly toward CaCo-2 and MCF-7 cells, highlights its potential for dual anti-inflammatory and anticancer activity, meriting further mechanistic exploration.

Computational studies

Molecular docking and binding energy analysis of pyrazole-carboxamides in COX isoenzymes

To complement the in vitro COX inhibition data and provide mechanistic insights into selectivity, molecular docking studies were performed using the XP-Glide protocol within the Schrödinger Maestro suite. Molecular docking was performed to predict the binding modes of compounds **3b**, **3d**, **3g**, and ketoprofen within COX-1 and COX-2. Crystal structures of COX-1 (PDB ID: 3KK6) and COX-2 (PDB ID: 5KIR) were selected due to their resolution quality and prior validation in selective NSAID docking studies. Docking scores, MM-GBSA binding free energies (ΔG), and key molecular interactions were analyzed to interpret the observed biological activity and selectivity (summarized in Table 2). The docking poses within the COX-1 and COX-2 binding sites are illustrated in Figs. 7 and 8, respectively. Among the tested compounds, the reference drug ketoprofen demonstrated the strongest binding affinity toward both COX-1 (docking score: −9.185 kcal/mol; ΔG: −49.87 kcal/mol) and COX-2 (−8.651 kcal/mol; ΔG: −60.59 kcal/mol), consistent with its potent in vitro inhibition of both isozymes.

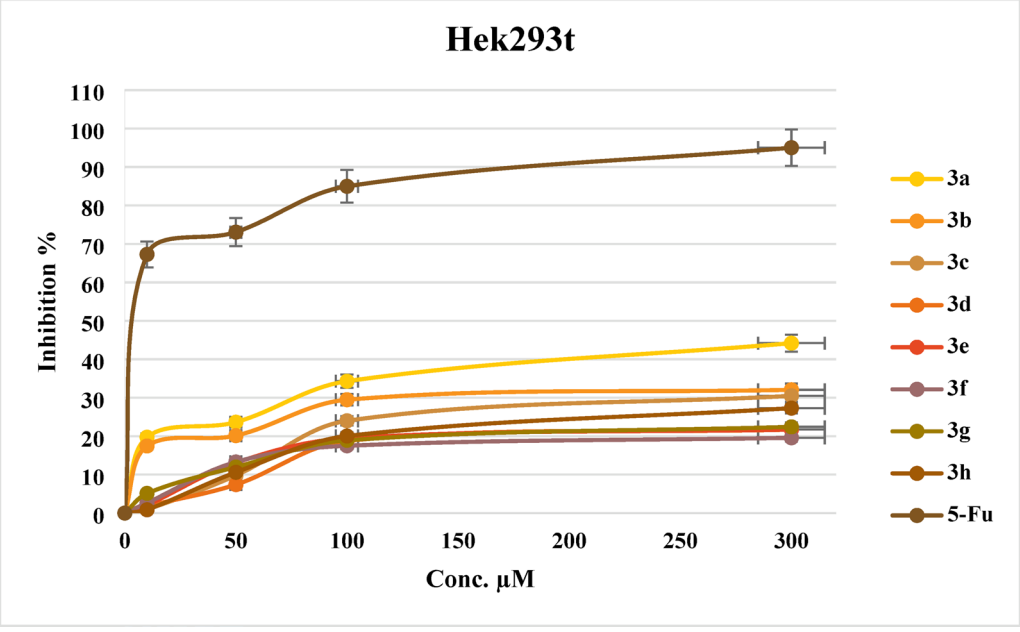

Fig. 4 Inhibition percentage of pyrazole-carboxamide derivatives (**3a**–**3h**) using Hek293t cells in comparison to the positive control 5-FU

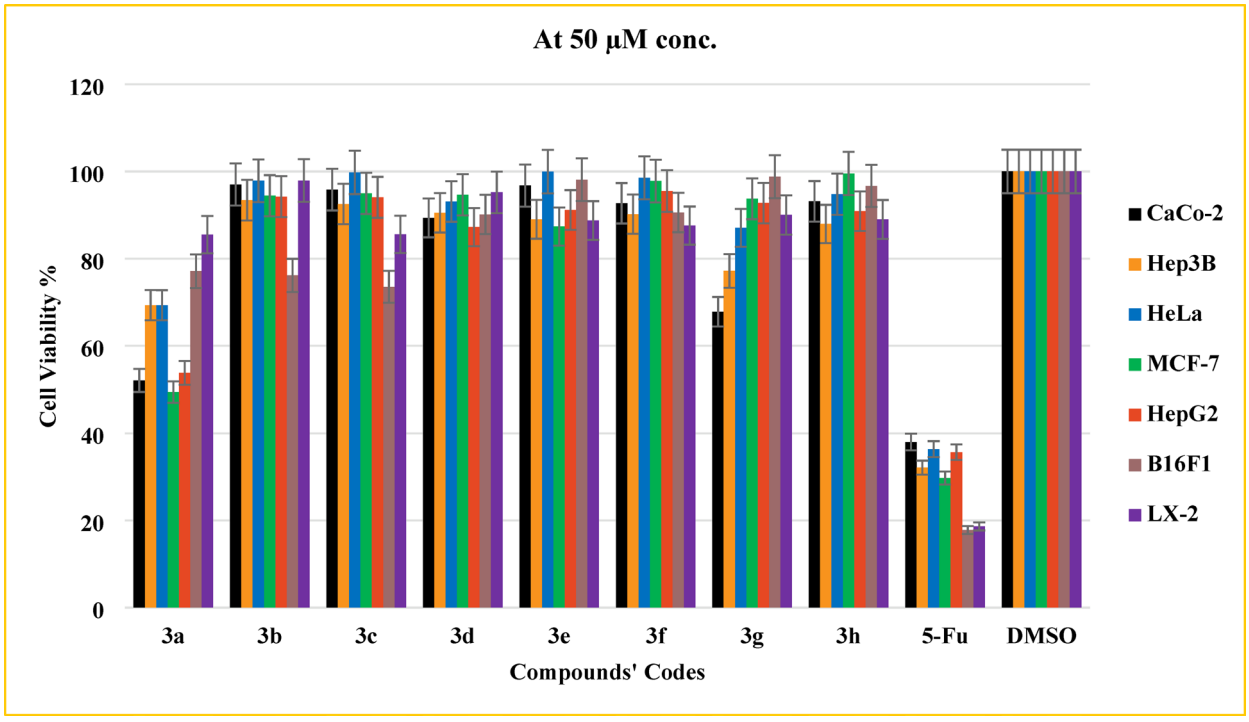

Fig. 5 Inhibition percentages of pyrazole–carboxamide derivatives (**3a**–**3h**) against various cell lines, compared to the positive control 5-fluorouracil (5-FU)

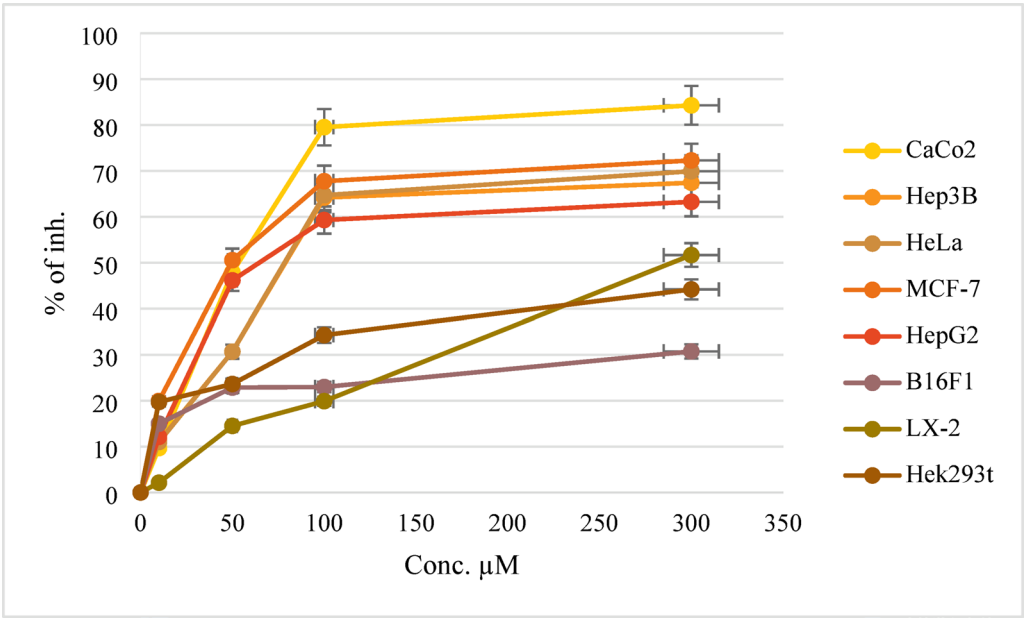

Fig. 6 Inhibition percentage of compound **3a** using various cancer and normal cell lines

As shown in Fig. 7D, ketoprofen within the COX-1 binding site established a hydrogen bond with R120, supported by extensive hydrophobic contacts with V349, L352, Y355, L359, Y385, W387, F518, and A527. In contrast, Fig. 8D shows its COX-2 binding mode, where it formed two hydrogen bonds with R120 and Y355, alongside multiple hydrophobic interactions with V349, Y355, L359, W387, F518, V523, and V527. These more pronounced interactions in COX-1 explain its lower COX-2/COX-1 selectivity ratio (0.21) and confirm its non-selective inhibitory profile. The docking profiles of compound **3b** are shown in Figs. 7A and 8A for COX-1 and COX-2, respectively. Compound **3b** exhibited strong affinity toward COX-1, with a docking score of − 5.066 kcal/mol

Table 2 Docking profiles of the synthesized ligands against COX-1 and COX-2 enzymes:

Ligand	COX	H. Bs	HPHO	π-Cationic	π-π stacking	Halogen bond	Docking score (Kcal/mol)	MM-GBSA (ΔG)
3b	COX-1	R120, Y355	I89, V116, R120, V349, L352, Y355, A527			I523	-5.066	-41.91
	COX-2	R120, Y355	V89, L93, V116, V349, L352, A527		Y355		-6.183	-36.80
3d	COX-1	R83	R79, L82, I89				-2.485	-27.56
	COX-2	R120, Y355	L93, V116, V349, L352, A527		Y355		-5.356	-35.61
3 g	COX-1		I89, L92, L112, V119, R120, L123	R120			-4.203	-36.22
	COX-2	R120 Y355	L93, W100, I112, Y115, V116, V349, Y355, L359, V523, A527		Y355		-7.135	-58.39
Ketoprofen	COX-1	R120, Y355	V349, L352. Y355, L359, Y385, W387, F518, A527				-9.185	-60.59
	COX-2	R120, Y355	V349, Y355, L359, W387, F518, V523, A527		W387		-8.651	-49.68

H. Bs Hydrogen bonds, *HPHO* hydrophobic interactions

and ΔG of − 41.91 kcal/mol, consistent with its potent in vitro COX-1 inhibition (IC_{50} = 0.46 μM). Its weaker activity against COX-2 (IC_{50} = 3.82 μM) and low selectivity ratio (0.12) indicate a COX-1–biased inhibition profile. In both enzymes, **3b** formed hydrogen bonds with R120 and Y355, as well as hydrophobic interactions involving V349, L352, and A527. Notably, in COX-1, **3b** established a unique halogen bond with I523, which likely contributes to its enhanced stabilization and preferential affinity for COX-1.

Compound **3g** demonstrated a significantly stronger binding affinity for COX-2 (docking score: − 7.135 kcal/mol; ΔG: − 58.39 kcal/mol) than for COX-1 (−4.203 kcal/mol; ΔG: − 36.22 kcal/mol), aligning with its in vitro potency (IC_{50} = 2.56 μM for COX-2) and highest selectivity ratio (1.68) among the series. In COX-1 (Fig. 7B), **3g** established limited polar contacts, while in COX-2 (Fig. 8B) it formed key hydrogen bonds with R83, Y355, W100, and Y115, together with π–π stacking and hydrophobic interactions with V349, L359, and A527. These interactions are well suited to the enlarged and more flexible COX-2 active site, supporting its selective inhibition.

Compound **3d** displayed moderate binding affinities toward COX-1 (docking score: − 2.485 kcal/mol; ΔG: − 27.56 kcal/mol) and COX-2 (−5.356 kcal/mol; ΔG: − 35.61 kcal/mol). This correlates with its relatively weaker in vitro inhibition (IC_{50} = 5.59 μM for COX-1 and 4.92 μM for COX-2) and intermediate selectivity ratio (1.14). In COX-1 (Fig. 7C), **3d** formed a single hydrogen bond with R120, whereas in COX-2 (Fig. 8C), it engaged R120 and Y355, supported by hydrophobic contacts with L93, V116, and V349. These features explain its modest preference for COX-2.

Overall, the molecular docking results strongly support the experimental findings, particularly in explaining the observed selectivity trends. Compounds **3b** and **3g** showed favorable binding interactions with COX-1 and COX-2, respectively, and their predicted poses and binding energies closely mirrored their in vitro IC_{50} values and selectivity profiles. Notably, the deep binding of compound **3g** within the expanded COX-2 pocket, stabilized by π–π and polar interactions, highlights its promise as a selective COX-2 inhibitor. In contrast, the chemical structure **3b** demonstrates a more non-selective binding mode, with greater affinity for COX-1.

In silico ADMET profiling of pyrazole-carboxamide derivatives

To assess the drug-likeness and pharmacokinetic feasibility of the synthesized compounds, in silico ADMET analyses were conducted using QikProp module of the Schrödinger suite. The pharmacokinetic profiles of the newly synthesized pyrazole–carboxamide derivatives were evaluated using a set of key in silico parameters, including predicted human oral absorption, aqueous solubility (QPlogS, which indicates the solubility of the compound in water and affects absorption and formulation potential), and blood–brain barrier penetration capability (QPlogBB, which predicts the likelihood of central nervous system exposure and helps assess potential CNS-related toxicity or off-target effects). Additionally, the compounds' likelihood of drug–drug interactions was estimated through their predicted binding affinity to human serum albumin (QPlogKhsa), while their potential cardiotoxicity was evaluated by predicting their ability to block HERG K^+ channels, a key indicator of arrhythmogenic risk. Together, these parameters provide a comprehensive overview of the compounds' pharmacokinetic behavior and help assess their suitability for progression into clinical development.

As summarized in Table 3, all synthesized trifluoromethyl–pyrazole–carboxamide derivatives demonstrated favorable ADME-T profiles, with each evaluated parameter falling within or close to the recommended ranges for drug-likeness. The molecular weights (Mw) ranged from 422 to 498 Da, aligning well with the preferred limits for orally active agents. Predicted human oral absorption (%) was consistently high, between 90 and 100%, suggesting

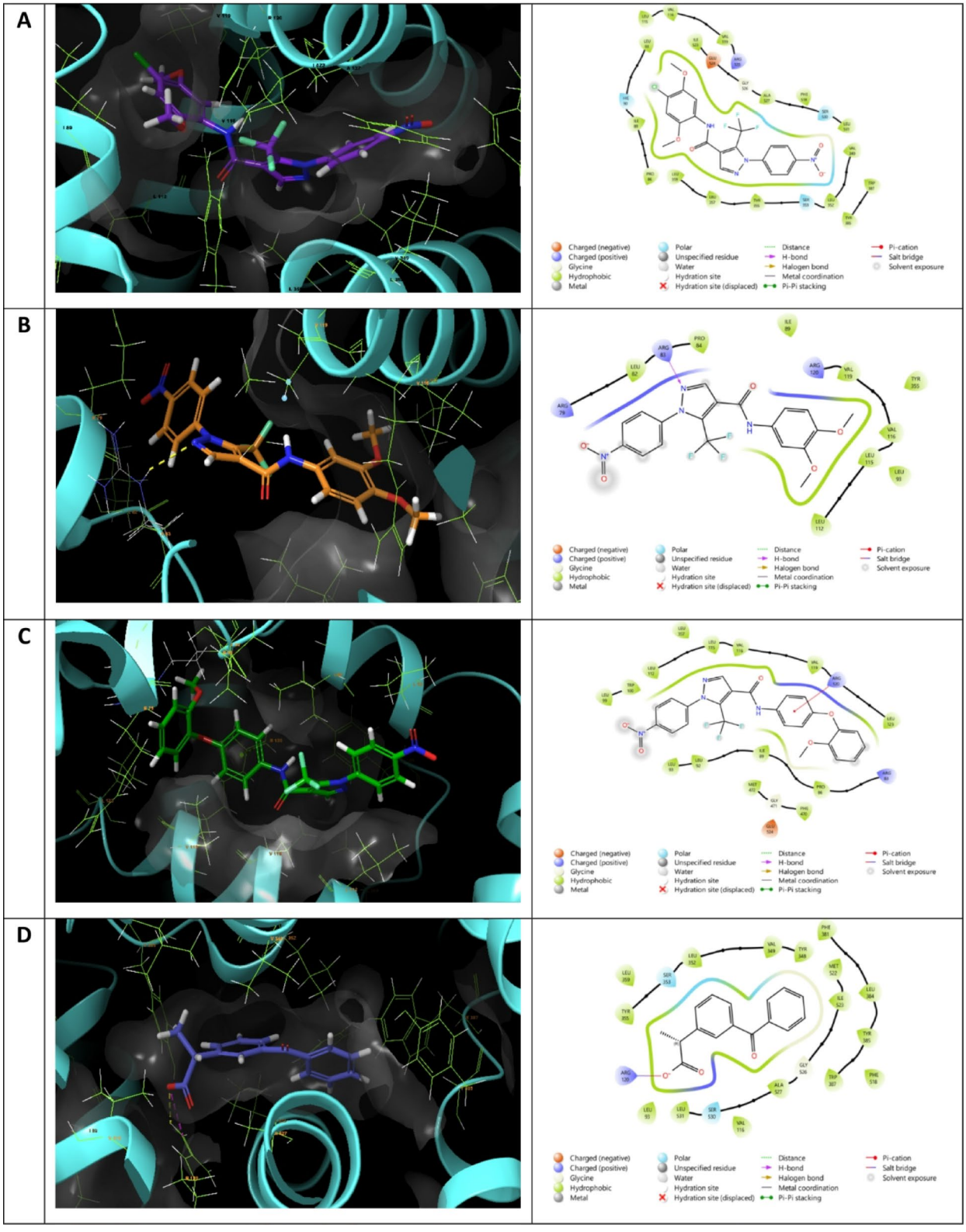

Fig. 7 Comparative docking poses of pyrazole–carboxamide derivatives and ketoprofen within the COX-1 binding site (PDB ID: 3KK6). Panels A–C correspond to compounds **3b**, **3 g**, and **3d**, respectively, while Panel D depicts the reference drug ketoprofen. Each panel shows both 2D and 3D interaction views

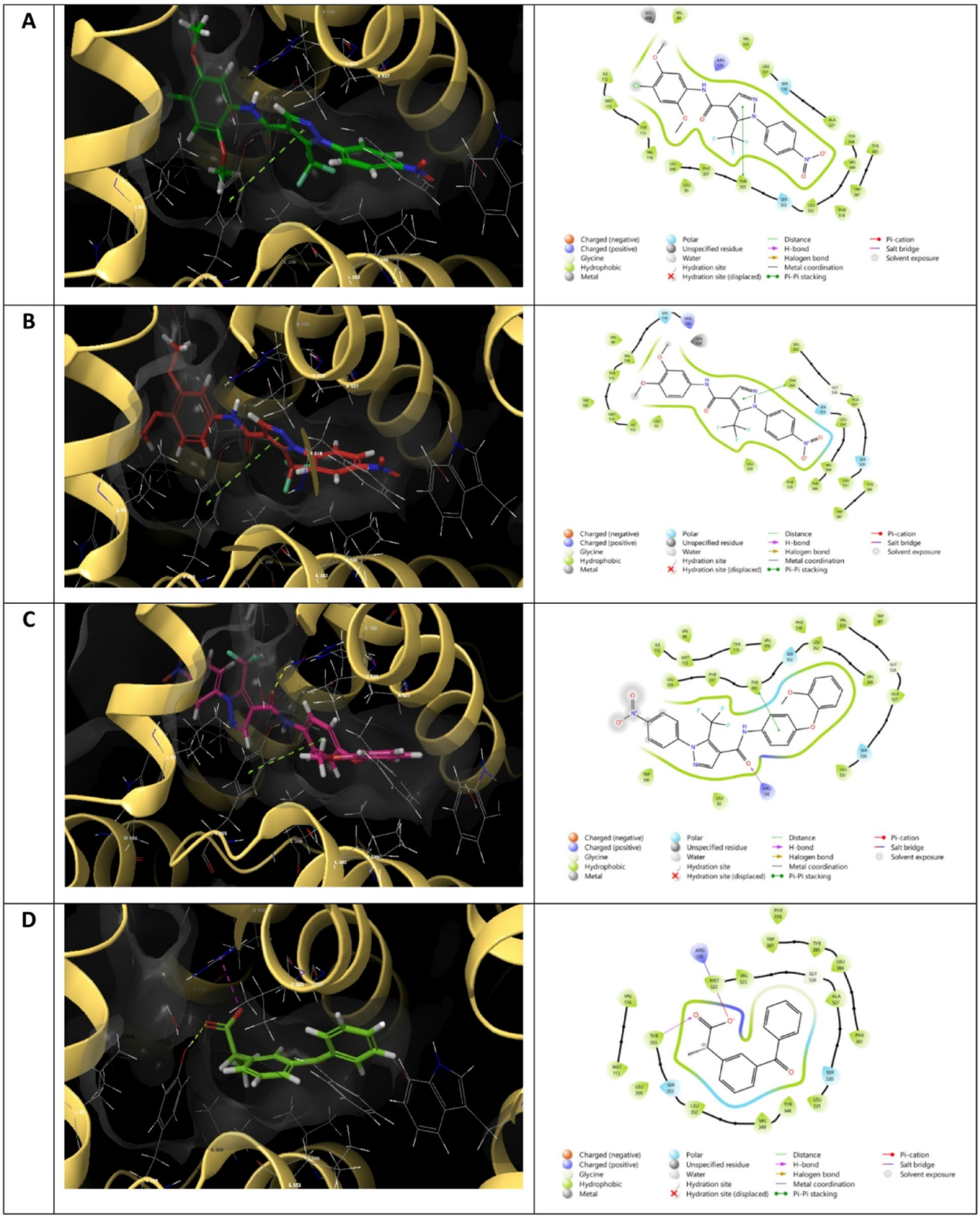

Fig. 8 Comparative docking poses of pyrazole–carboxamide derivatives and ketoprofen within the COX-2 binding site (PDB ID: 5KIR). Panels A–C correspond to compounds **3b**, **3 g**, and **3d**, respectively, while Panel D depicts the reference drug ketoprofen. Each panel presents both 2D and 3D interaction views

Table 3 ADME-T profiling of pyrazole–carboxamide derivatives (compounds **3a**–**3h**)

Compound	MW	Human Oral Absorption (%)	QPlogPo/w	QPlogS	QPlogBB	TPSA (Å²)	QPlogKhsa	QPPCaco	QPlogHERG	Lipinski rule violation; drug-likeness
3a	432.401	100.000	4.949	-7.263	-1.033	94.608	1.000	376.214	-6.145	0;Yes
3b	470.792	100.000	4.480	-6.969	-0.955	108.961	0.627	382.353	-6.057	0;Yes
3c	436.347	96.004	3.904	-6.062	-1.074	111.012	0.481	381.333	-6.013	0;Yes
3d	436.347	96.069	3.914	-6.100	-1.082	110.369	0.485	381.533	-6.049	0;Yes
3e	422.381	100.000	4.335	-6.610	-0.922	94.630	0.640	381.931	-6.271	0;Yes
3f	452.392	90.965	5.304	-7.631	-1.103	94.592	1.047	367.879	-7.388	1;Yes
3 g	498.417	91.415	5.405	-7.713	-1.273	108.958	0.996	361.155	-7.351	1;Yes
3 h	466.373	96.946	4.067	-6.324	-1.173	117.901	0.509	380.687	-5.963	0;Yes
Recommended values	**130–725**	**> 80% is high, < 25% is low**	**-2.0-6.5**	**-6.0-0.5**	**-3–1.2**	**90–140**	**-1.5–1.5**	**< 25 poor > 500 great**	**>-5**	**Less than 2, yes**

excellent gastrointestinal bioavailability. The lipophilicity values (QPlogPo/w) fell within the range of 3–5, indicating a balanced hydrophilic–lipophilic profile favorable for membrane permeability, while aqueous solubility (QPlogS) a little bit exceeded the normal range (-6 to 0.5) but still in the acceptable range of (–6 to – 7), supporting adequate solubility for oral administration.

Predicted blood–brain barrier penetration (QPlogBB) values were approximately – 1, indicating limited CNS exposure, which is beneficial for reducing potential off-target central nervous system effects. The topological polar surface area (TPSA) ranged from 94 to 117 Å², consistent with favorable absorption and bioavailability. Protein-binding potential, assessed via QPlogKhsa, was in the range of 0.4–1, suggesting appropriate plasma protein interactions without excessive sequestration. Predicted Caco-2 cell permeability (QPPCaco) values ranged from 361 to 382, indicating high intestinal permeability. Cardiotoxicity risk, evaluated through QPlogHERG values, was low (–5 to – 7), reflecting minimal likelihood of HERG channel blockade.

All compounds satisfied Lipinski's rule of five with zero or only one violation, further supporting their oral drug-likeness. Collectively, these ADMET parameters indicate that the synthesized derivatives possess favorable pharmacokinetic characteristics, low toxicity risk, and suitable drug-like properties, justifying their further optimization and preclinical evaluation.

Molecular weight (Mol._Mw), octanol/water partition coefficient (QPlogPo/w), aqueous solubility (QPlogS), brain/blood partition coefficient (QPlogBB), the ability to cross the blood-brain barrier (QPlogBB), the total polar surface area (TPSA), the binding affinity to human serum albumin (QPlogKhsa), Caco-2 cell permeability in nm/sec, and QPlogHERG that predicts the IC50 value for blockage of HERG K + channels.

SAR analysis

To rationalize the observed inhibitory activities and selectivity indices, a detailed SAR analysis was performed based on the electronic and steric properties of the substituents. The structure–activity relationship (SAR) analysis of the newly synthesized pyrazole–carboxamide derivatives revealed several critical factors influencing COX-1 and COX-2 inhibitory activity and selectivity. The incorporation of a trifluoromethyl group onto the pyrazole ring significantly enhanced hydrophobic stabilization within the COX binding pockets, contributing to increased ligand–receptor affinity. Additionally, the electron-rich pyrazole moiety facilitated favorable π–π stacking and π–π-cation interactions with key aromatic and charged residues, improving the anchoring and binding strength of the ligands. Furthermore, the introduction of nitrophenyl substituents mimicked, to some extent, the sulfonamide-phenyl groups found in FDA-approved COX-2 inhibitors such as celecoxib, assisting in proper orientation within the COX-2 side pocket and promoting favorable conformational stability and selectivity.

The presence of the trifluoromethyl group enhanced hydrophobic stabilization and contributed to increased binding affinity across both isoforms. The para-chloro group in compound **3b** likely contributed to enhanced COX-1 affinity through halogen bonding interactions, consistent with its low selectivity index.

Regarding phenyl ring substitution patterns, derivatives bearing weak electron-donating groups such as tert-butyl (compound **3a**), methylthio (compound **3e**), and phenyl (compound **3f**) at the para position exhibited relatively poor inhibitory activities against both COX-1 and COX-2, supporting previous findings that these groups provide stability but do not significantly enhance potency or selectivity. In contrast, the introduction of strong electron-donating methoxy groups at the meta positions (3,5-dimethoxy in compound **3c**) improved inhibitory potency. Expanding the substitution to include both meta and para positions (3,4,5-trimethoxy in compound

3h) further enhanced activity, particularly against COX-2, when compared to compounds with fewer methoxy groups (e.g., compound **3d**, 3,4-dimethoxy). The introduction of methoxy substituents at various positions on the aryl ring increased COX-2 selectivity, with 3,4,5-trimethoxy (compound **3h**) exhibiting more favorable activity than di-substituted analogues.

However, the most potent COX-1 inhibitor was compound **3b**, which combined methoxy groups at ortho and meta positions with a chlorine atom at the para position. The chloro substituent likely enhanced COX-1 binding affinity through favorable halogen bonding, consistent with earlier studies highlighting the beneficial role of halogens in COX-1 targeting [52]. Compound **3b** demonstrated strong inhibitory activity against COX-1 (IC_{50} = 0.46 ± 0.25 μM) and moderate inhibition against COX-2 (IC_{50} = 3.82 ± 1.36 μM), but with a lower selectivity index (SI = 0.12), suggesting non-preferential COX-2 inhibition.

In contrast, compound **3g**, featuring a bulky 2-methoxyphenoxy group, exhibited the highest COX-2 selectivity (SI = 1.68), exceeding the selectivity of the reference drug ketoprofen (SI = 0.21). The bulkiness of the methoxyphenoxy group likely promotes optimal fitting within the larger COX-2 side pocket while restricting access to the smaller COX-1 pocket, supporting reports that bulky substituents enhance COX-2 selectivity [1]. The oxygen linker also contributes to the electronic donation and spatial orientation, enabling favorable alignment within the COX-2 binding domain.

Additionally, compounds **3f** (4-aminobiphenyl) and **3h** (3,4,5-trimethoxy) demonstrated favorable selectivity indices (0.98 and 0.93, respectively), further supporting the idea that bulky, electron-donating substituents enhance COX-2 selectivity. Structural comparisons among dimethoxy-substituted derivatives revealed that compound **3d** (3,4-dimethoxy) exhibited a better selectivity index (SI = 1.14) compared to compound **3c** (3,5-dimethoxy), highlighting the influence of substitution position on enzyme selectivity. This trend is consistent with previous observations that methoxy substituents positioned at meta and para sites can enhance COX-2 binding affinity [53].

Overall, these SAR findings emphasize the crucial roles of hydrophobicity, electronic effects, substituent size, steric factors, and positioning in modulating the potency and isoform selectivity of the pyrazole–carboxamide scaffold. These findings highlight the importance of fine-tuning electronic and steric features to optimize COX isoform selectivity, a key goal in designing safer anti-inflammatory agents.

Conclusion

In this work, a series of trifluoromethyl-substituted pyrazole–carboxamide derivatives was designed, synthesized, and comprehensively evaluated with the primary objective of developing selective COX-2 inhibitors with favorable safety and drug-like properties. Several compounds, particularly **3d** and **3g**, exhibited potent COX-2 inhibition with high selectivity indices and minimal activity against COX-1, indicating their promise as safer anti-inflammatory agents. Structural validation of selected derivatives via MicroED provided atomic-level confirmation of the molecular architecture, supporting the observed structure–activity relationships. Furthermore, the compounds demonstrated low cytotoxicity against non-tumorigenic HEK293T and LX-2 cell lines, while select molecules showed moderate antiproliferative effects on CaCo-2 and HepG2 cells, suggesting potential dual anti-inflammatory and anticancer profiles. In silico ADMET predictions further corroborated the favorable pharmacokinetic and safety characteristics, with all compounds meeting key drug-likeness criteria and displaying low predicted cardiotoxicity risks. Molecular docking and MM-GBSA binding energy analyses further explained the observed COX-2 selectivity through favorable binding orientations and interactions within the COX-2 active site. Overall, this study successfully identified promising COX-2–selective candidates with favorable pharmacological and safety profiles, thereby achieving its stated objective and providing a strong foundation for further in vivo validation and translational development.

Supplementary Information

The online version contains supplementary material available at https://doi.org/10.1186/s13065-025-01659-z.

Supplementary Material 1.

Acknowledgements

The authors would like to thank An-Najah National University (www.najah.edu), Gazi University for their support in chemical analysis. Acknowledgment is also extended to the Cryomicroscopy and Electron Diffraction Core Facility at the Centre of New Technologies, University of Warsaw, for granting access to the 3DED infrastructure. Additionally, the National Science Center, Poland, provided the funding for AK, BO and PMD under the grant 2020/39/I/ST4/02904.

Author contributions

M.H. M.T.Q. and N.S. Writing – review & editing, Writing – original draft, Visualization, Validation, Supervision, Methodology, Formal analysis, Data curation, Conceptualization. I.Ç. Writing, Validation, Formal analysis (NMR and HRMS). M.A. Methodology COX analysis. A.K., B.A. and P.M.D. Investigation, Formal analysis, Data curation of MicroED.

Funding

None.

Data availability

All data generated or analysed during this study are included in this published article (and its supplementary information files). Additional crystallographic details related to this study are accessible via CCDC entries 2455616-2455618.

These data can be freely obtained at www.ccdc.cam.ac.uk/data_request/cif or by emailing [data_request@ccdc.cam.ac.uk](mailto: data_request@ccdc.cam.ac.uk) . Alternatively, the Cambridge Crystallographic Data Centre can be contacted at 12 Union Road, Cambridge CB2 1EZ, UK, or via fax at + 44 1223 336033.

Declarations

Ethics approval and consent to participate
Not applicable.

Consent for publication
The authors of the current work gave constant for publication to Dr. Mohammed Hawash.

Competing interests
The authors declare no competing interests.

Author details
[1]Department of Pharmaceutical Chemistry and Technology, Faculty of Pharmacy, Faculty of Medicine and Health Sciences, An-Najah National University, Nablus, Palestine
[2]Department of Pharmacy, Faculty of Pharmacy, Cyprus International University, Northern Cyprus, Mersin 10, 99258 Nicosia, Türkiye
[3]Department of Pharmaceutical Basic Sciences, Faculty of Pharmacy, Gazi University, 06330 Ankara, Turkey
[4]Sente Kimya Research and Development Inc, 06200 Ankara, Turkey
[5]Faculty of Chemistry, Biological and Chemical Research Centre, University of Warsaw, 02-089 Warsaw, Poland

Received: 7 June 2025 / Accepted: 2 October 2025
Published online: 29 October 2025

References

1. Chamakuri K, Muppavarapu SM, Yellu NR. Synthesis, characterization, and Pharmacological evaluation of some novel hydrazone derivatives derived from 3-((4-formyl-2-methoxyphenoxy) methyl) benzonitrile. Int J Pharm Sci Res. 2016;7(4):1633.
2. Simmons DL, Botting RM, Hla T. Cyclooxygenase isozymes: the biology of prostaglandin synthesis and Inhibition. Pharmacol Rev. 2004;56(3):387–437.
3. Mahto K, Kuwar OK, Maloo A, Kumar A. Therapeutic potential of Boswellia Serrata in arthritis management: mechanistic insights into COX-2, 5-LOX, and NFκB modulation. Inflammopharmacology 2025;33:5085–96. https://doi.org/10.1007/s10787-025-01912-w
4. Miciaccia M, Belviso BD, Iaselli M, Cingolani G, Ferorelli S, Cappellari M, Loguercio Polosa P, Perrone MG, Caliandro R, Scilimati A. Three-dimensional structure of human cyclooxygenase (h COX)-1. Sci Rep. 2021;11(1):4312.
5. Agrawal N. A comprehensive review on the advancements of dual COX-2/5-LOX inhibitors as Anti-Inflammatory drugs. Chem Biol Drug Des. 2025;105(5):e70114.
6. Ali KA, Maity A, Roy SD, Pramanik SD, Das PP, Shaharyar MA. Insight into the mechanism of steroidal and non-steroidal anti-inflammatory drugs. In: *How Synthetic Drugs Work*. Elsevier; 2023: 61–94.
7. Sharma K, Kumar D, Chandna N, Kapoor JK. Celecoxib Reimagined: Multifunctional Roles in Advanced Drug Delivery and Therapeutics. *ChemistrySelect* 2025, 10(31):e02652.
8. Liu Y, Yang C, Zhang J, Ihsan A, Ares I, Martínez M, Lopez-Torres B, Martínez-Larrañaga M-R, Wang X, Anadón A. Recent progress in adverse events of carboxylic acid non-steroidal anti-inflammatory drugs (CBA-NSAIDs) and their association with the metabolism: the consequences on mitochondrial dysfunction and oxidative stress, and prevention with natural plant extracts. Expert Opin Drug Metab Toxicol. 2024;20(8):765–85.
9. Evren AE, Kaya AZ, Karakaya A, Tutuş B, Güngör EM, Nuha D, Osmaniye D, Kaya B, Çevik UA, Yurttaş L. Latest developments in small molecule analgesics: heterocyclic scaffolds I. Future Med Chem 2025;17(15):1899–918. https://doi.org/10.1080/17568919.2025.2546783
10. Perrone MG, Vitale P, Panella A, Fortuna CG, Scilimati A. General role of the amino and Methylsulfamoyl groups in selective cyclooxygenase (COX)-1 Inhibition by 1, 4-diaryl-1, 2, 3-triazoles and validation of a predictive pharmacometric PLS model. Eur J Med Chem. 2015;94:252–64.
11. Kolb HC, Finn M, Sharpless KB. Click chemistry: diverse chemical function from a few good reactions. Angew Chem Int Ed. 2001;40(11):2004–21.
12. Altaf AA, Shahzad A, Gul Z, Rasool N, Badshah A, Lal B, Khan E. A review on the medicinal importance of pyridine derivatives. J Drug Des Med Chem. 2015;1(1):1–11.
13. Assali M, Abualhasan M, Sawaftah H, Hawash M, Mousa A. Synthesis, biological Activity, and molecular modeling studies of pyrazole and Triazole derivatives as selective COX-2 inhibitors. J Chem. 2020;2020(1):6393428.
14. Ansari A, Ali A, Asif M. Biologically active pyrazole derivatives. New J Chem. 2017;41(1):16–41.
15. Perrone MG, Vitale P, Panella A, Ferorelli S, Contino M, Lavecchia A, Scilimati A. Isoxazole-based-scaffold inhibitors targeting cyclooxygenases (COXs). ChemMedChem. 2016;11(11):1172–87.
16. Rayar AM, Lagarde N, Martin F, Blanchard F, Liagre B, Ferroud C, Zagury J-F, Montes M. Veitía MS-I: new selective cyclooxygenase-2 inhibitors from cyclocoumarol: Synthesis, characterization, biological evaluation and molecular modeling. Eur J Med Chem. 2018;146:577–87.
17. Khan Z, Khan N, Tiwari P, Sah RK, Prasad N, Bisen GS. Biology of Cox-2: an application in cancer therapeutics. Curr Drug Targets. 2011;12(7):1082–93.
18. Ghosh N, Chaki R, Mandal V, Mandal SC. COX-2 as a target for cancer chemotherapy. Pharmacol Rep. 2010;62(2):233–44.
19. Khan HY, Parveen S, Yousuf I, Tabassum S, Arjmand F. Metal complexes of NSAIDs as potent anti-tumor chemotherapeutics: mechanistic insights into cytotoxic activity via multiple pathways primarily by Inhibition of COX–1 and COX–2 enzymes. Coord Chem Rev. 2022;453:214316.
20. Hawash M, Abdallah S, Abudayyak M, Melhem Y, Shamat MA, Aghbar M, Çapan I, Abualhasan M, Kumar A, Kamiński M. Exploration of isoxazole analogs: Synthesis, COX inhibition, anticancer screening, 3D multicellular tumor spheroids, and molecular modeling. Eur J Med Chem. 2024;271:116397.
21. Akhtar W, Marella A, Alam MM, Khan MF, Akhtar M, Anwer T, Khan F, Naematullah M, Azam F, Rizvi MA. Design and synthesis of pyrazole–pyrazoline hybrids as cancer-associated selective COX-2 inhibitors. Arch Pharm. 2021;354(1):2000116.
22. Abdellatif KR, Fadaly WA, Mostafa YA, Zaher DM, Omar HA. Thiohydantoin derivatives incorporating a pyrazole core: Design, synthesis and biological evaluation as dual inhibitors of topoisomerase-I and cycloxygenase-2 with anti-cancer and anti-inflammatory activities. Bioorg Chem. 2019;91:103132.
23. Mukarram S, Bandgar BP, Shaikh RU, Ganapure SD, Chavan HV. Synthesis of novel α, α-difluoro-β-hydroxycarbonyl pyrazole derivatives as antioxidant, anti-inflammatory and anticancer agents. Med Chem Res. 2017;26:262–73.
24. Deivasigamani P, Rubavathy SE, Jayasankar N, Saravanan V, Thilagavathi R, Prakash M, Selvam C, Rajagopal R, Alfarhan A, Kathiravan MK. Dual Anti-Inflammatory and anticancer activity of novel 1, 5-Diaryl pyrazole derivatives: molecular Modeling, Synthesis, in vitro activity, and dynamics study. Biomedicines. 2024;12(4):788.
25. Fadaly WA, Elshaier YA, Nemr MT, Abdellatif KR. Design, synthesis, modeling studies and biological evaluation of pyrazole derivatives linked to oxime and nitrate moieties as nitric oxide donor selective COX-2 and aromatase inhibitors with dual anti-inflammatory and anti-neoplastic activities. Bioorg Chem. 2023;134:106428.
26. Ahmed AH, Mohamed MF, Allam RM, Nafady A, Mohamed SK, Gouda AE, Beshr EA. Design, synthesis, and molecular Docking of novel pyrazole-chalcone analogs of Lonazolac as 5-LOX, iNOS and tubulin polymerization inhibitors with potential anticancer and anti-inflammatory activities. Bioorg Chem. 2022;129:106171.
27. Sebbar N, Ellouz M, Essassi E, Ouzidan Y, Mague J. Crystal structure of 4-benzyl-2H-benzo [b][1, 4] thiazin-3 (4H)-one. Acta Crystallogr Sect E: Crystallographic Commun. 2015;71(12):o999–999.
28. Dolomanov OV, Bourhis LJ, Gildea RJ, Howard JA, Puschmann H. OLEX2: a complete structure solution, refinement and analysis program. J Appl Crystallogr. 2009;42(2):339–41.
29. Chodkiewicz ML, Migacz S, Rudnicki W, Makal A, Kalinowski JA, Moriarty NW, Grosse-Kunstleve RW, Afonine PV, Adams PD, Dominiak PM. DiSCaMB: a software library for aspherical atom model X-ray scattering factor calculations with cpus and GPUs. J Appl Crystallogr. 2018;51(1):193–9.
30. Jha KK, Gruza B, Sypko A, Kumar P, Chodkiewicz ML, Dominiak PM. Multipolar atom types from theory and statistical clustering (MATTS) data bank: restructurization and extension of UBDB. J Chem Inf Model. 2022;62(16):3752–65.
31. Kleemiss F, Dolomanov OV, Bodensteiner M, Peyerimhoff N, Midgley L, Bourhis LJ, Genoni A, Malaspina LA, Jayatilaka D, Spencer JL. Accurate

crystal structures and chemical properties from NoSpherA2. Chem Sci. 2021;12(5):1675–92.
32. Gruza B, Chodkiewicz ML, Krzeszczakowska J, Dominiak PM. Refinement of organic crystal structures with multipolar electron scattering factors. Acta Crystallogr Sect A: Found Adv. 2020;76(1):92–109.
33. Hawash M, Al-Smadi D, Kumar A, Olech B, Dominiak PM, Jaradat N, Antari S, Mohammed S, Nasasrh Aa, Abualhasan M. Characterization and investigation of novel benzodioxol derivatives as antidiabetic agents: an in vitro and in vivo study in an animal model. Biomolecules. 2023;13(10):1486.
34. Hawash M, Jaradat N, Abualhasan M, Amer J, Levent S, Issa S, Ibrahim S, Ayaseh A, Shtayeh T, Mousa A. Synthesis, chemo-informatics, and anticancer evaluation of fluorophenyl-isoxazole derivatives. Open Chem. 2021;19(1):855–63.
35. Chaudhary KK, Mishra N. A review on molecular docking: novel tool for drug discovery. Databases. 2016;3(4):1029.
36. Hawash M, Jaradat N, Sabobeh R, Abualhasan M, Qaoud MT. New thiazole Carboxamide derivatives as COX inhibitors: Design, Synthesis, anticancer Screening, in Silico molecular Docking, and ADME profile studies. ACS Omega. 2023;8(32):29512–26.
37. Hawash M, Jaradat N, Abualhasan M, Şüküroğlu MK, Qaoud MT, Kahraman DC, Daraghmeh H, Maslamani L, Sawafta M, Ratrout A. Design, synthesis, molecular Docking studies and biological evaluation of thiazole Carboxamide derivatives as COX inhibitors. BMC Chem. 2023;17(1):11.
38. Hawash M, Jaradat N, Abualhasan M, Qaoud MT, Joudeh Y, Jaber Z, Sawalmeh M, Zarour A, Mousa A, Arar M. Molecular Docking studies and biological evaluation of isoxazole-carboxamide derivatives as COX inhibitors and antimicrobial agents. 3 Biotech. 2022;12(12):1–16.
39. Rimon G, Sidhu RS, Lauver DA, Lee JY, Sharma NP, Yuan C, Frieler RA, Trievel RC, Lucchesi BR, Smith WL. Coxibs interfere with the action of aspirin by binding tightly to one monomer of cyclooxygenase-1. *Proceedings of the National Academy of Sciences* 2010, 107(1):28–33.
40. Bhor RJ, Wani SV, Thorat KA, Sadaphal OB, Varpe TR, Ghogare PV, Bhosle SG, Gadekar SS. Computational simulation of COX-1 (PDB: 3KK6) and COX-2 (PDB: 3LN1) enzyme: 3D-QSAR Study, Docking molecular and simulation dynamic on series of benzimidazole derivatives. Asian J Biol Life Sci. 2025;14(2):1–11.
41. Pal M, Shukla R, Maurya A, Siddiqui Z, Srivastava R, Pathak SK, Shukla VK, Prasad O, Sinha L. In Silico insights into dual COX Inhibition by fluoro-substituted Indole derivative using DFT, molecular docking, and MD simulation studies. J Chin Chem Soc.2025;72(6);653–76. https://doi.org/10.1002/jccs.70020
42. Schake P, Bolz SN, Linnemann K, Schroeder M. PLIP 2025: introducing protein–protein interactions to the protein–ligand interaction profiler. Nucleic Acids Res. 2025;53(W1):463–5. https://doi.org/10.1093/nar/gkaf361
43. Bolz SN, Schake P, Stitz C, Schroeder M. The structural basis of drugs targeting protein-protein interactions uncovered with the protein-ligand interaction profiler PLIP. *Expert Opinion on Drug Discovery* 2025(just-accepted).
44. Adasme MF, Linnemann KL, Bolz SN, Kaiser F, Salentin S, Haupt VJ, Schroeder M. PLIP 2021: expanding the scope of the protein–ligand interaction profiler to DNA and RNA. Nucleic Acids Res. 2021;49(W1):W530–4.
45. Salentin S, Schreiber S, Haupt VJ, Adasme MF, Schroeder M. PLIP: fully automated protein–ligand interaction profiler. Nucleic Acids Res. 2015;43(W1):W443–7.
46. Li B, Xie F, Zhang R, Wang Y, Gondi VB, Hale CR. Synthesis of diverse N-Trifluoromethyl pyrazoles by trapping of Transiently-Generated trifluoromethylhydrazine. J Org Chem. 2024;89(19):13959–69.
47. Kaur K, Kumar V, Gupta GK. Trifluoromethylpyrazoles as anti-inflammatory and antibacterial agents: A review. J Fluorine Chem. 2015;178:306–26.
48. Chahal S, Rani P, Kiran, Sindhu J, Joshi G, Ganesan A, Kalyaanamoorthy S, Mayank, Kumar P, Singh R. Design and development of COX-II inhibitors: current scenario and future perspective. ACS Omega. 2023;8(20):17446–98.
49. Penning TD, Talley JJ, Bertenshaw SR, Carter JS, Collins PW, Docter S, Graneto MJ, Lee LF, Malecha JW, Miyashiro JM. Synthesis and biological evaluation of the 1, 5-diarylpyrazole class of cyclooxygenase-2 inhibitors: identification of 4-[5-(4-methylphenyl)-3-(trifluoromethyl)-1 H-pyrazol-1-yl] benzenesulfonamide (SC-58635, celecoxib). J Med Chem. 1997;40(9):1347–65.
50. Limongelli V, Bonomi M, Marinelli L, Gervasio FL, Cavalli A, Novellino E, Parrinello M. Molecular basis of cyclooxygenase enzymes (COXs) selective Inhibition. Proc Natl Acad Sci. 2010;107(12):5411–6.
51. Blobaum AL, Uddin MJ, Felts AS, Crews BC, Rouzer CA, Marnett LJ. The 2′-trifluoromethyl analogue of indomethacin is a potent and selective COX-2 inhibitor. ACS Med Chem Lett. 2013;4(5):486–90.
52. Shtamburg VG, Tsygankov AV, Shishkin OV, Zubatyuk RI, Uspensky BV, Shtamburg VV, Mazepa AV, Kostyanovsky RG. The properties and structure of N-chloro-N-methoxy-4-nitrobenzamide. Mendeleev Commun. 2012;22(3):164–6.
53. Bergin E. Substituting methoxy groups. Nat Chem. 2014;6(11):947–947.

Publisher's note